ARMY RESEARCH LABORATORY

Performance Bounds on Atmospheric Acoustic Sensor Arrays Operating in a Turbulent Medium I. Plane-Wave Analysis

Sandra L. Collier and D. Keith Wilson

ARL-TR-2426

February 2002

The findings in this report are not to be construed as an official Department of the Army position unless so designated by other authorized documents.

Citation of manufacturer's or trade names does not constitute an official endorsement or approval of the use thereof.

Destroy this report when it is no longer needed. Do not return it to the originator.

Army Research Laboratory

Adelphi, MD 20783-1197

ARL-TR-2426 February 2002

Performance Bounds on Atmospheric Acoustic Sensor Arrays Operating in a Turbulent Medium I. Plane-Wave Analysis

Sandra L. Collier and D. Keith Wilson

Computational and Information Sciences Directorate

Abstract

The performance bounds of an atmospheric acoustic array operating in a turbulent medium with fluctuations described by a von Kármán spectrum are investigated. This treatment considers a single monochromatic source and a line-of-sight propagation path. The primary interests are in calculating the Cramer-Rao lower bounds (CRLBs) of the azimuthal and zenith angles of arrival (AOAs) and in observing how these bounds change with the introduction of additional unknowns, such as the normalized propagation distance (to wavelength), turbulence parameters, and signal-to-noise ratio (SNR). In both two and three dimensions, the CRLBs of the AOAs increase significantly for large values of the index-of-refraction variance and normalized propagation distance. For small values of the index-of-refraction variance and normalized propagation distance, the SNR is the limiting factor. For the two-dimensional treatment, the estimate of the AOA will decouple from the estimates of the other parameters with the appropriate choice of array geometry. In three dimensions, again with an appropriate choice of array geometry, the estimates of the azimuth and zenith will decouple from the estimates of the other parameters, but because of the constraints of the turbulence model, they will remain coupled to one another.

Contents

Figures

1. Introduction

Acoustical direction-finding and tracking systems will likely play a prominent role on the future battlefield, where situational awareness will be a key factor affecting the survivability of light- and medium-weight forces. The main advantages of acoustical sensors are low cost, small size, passive operation, and operational capabilities in non-line-of-sight (non-LOS) conditions. However, the performance of acoustical sensors does strongly depend on environmental conditions.

This report discusses how one important environmental effect, the scattering of sound, affects the ability of arrays of acoustical sensors to determine the bearing angles of targets. Scattering occurs when sound interacts with turbulence and other random atmospheric motions, creating random distortions in the propagating wavefronts. As the wavefronts propagate from the source (target) to the receiving array, they can accumulate substantial random variations in their orientation and intensity, which are perceived as fluctuations in the apparent bearing angles and strength of the source. These acoustic phenomena are analogous to scintillation and quivering of optical images, as are often observed above a roadway on a sunny afternoon.

The study of the scattering of waves propagating in a random medium is already well established. Only recently, however, have researchers begun to directly incorporate the effects of the scattering into performance predictions for acoustic direction-finding arrays. Accounting for the strong distortion of the wavefront by atmospheric turbulence is crucial to obtaining accurate performance characterization.

The performance of a sensor array may be quantified by calculating the mean square error (MSE) between the estimated parameter (such as the angle of arrival (AOA) or propagation distance) and its actual value. The lower bound of the MSE is the Cramer-Rao lower bound (CRLB), which is calculated from the Fisher information (FI). An approach that directly incorporated the effects of a random medium into the calculation of the FI was first formulated by Song and Ritcey [1] to calculate the performance bounds of AOA* estimates for ocean acoustics. Using the general

*In this report we make a distinction between the AOAs of the sound wave at the array and the actual angles of bearing (AOB) of the source. The theoretical treatment in this re-

framework of Song and Ritcey [1], Wilson [2] calculated the performance bounds on AOA estimates for atmospheric acoustic arrays.

The analysis by Song and Ritcey [1] considered the effects of a random medium, characterized by a fluctuation strength, on the performance of a linear acoustic array. The total received signal was taken to be that from multiple, uncorrelated, plane-wave source signals and from noise. They assumed that both the signal component and the noise component had a Gaussian distribution with zero mean. The covariance matrix for the source was calculated from the second moment of the sound field as predicted by the theory of waves propagating in a random medium. For no noise, they found a non-negligible change in the CRLB of the AOA for increasing fluctuation strength. For a fixed fluctuation strength and unknown noise parameter, they found that the CRLB of the AOA decreased as the signal-to-noise ratio (SNR) increased. A maximum likelihood estimator (MLE) was used and compared to the CRLB: the MLE was usually well within 20 percent of the CRLB for five independent data sets. The authors also noted that the estimator calculated from a beamforming method with the use of a Bartlett processor was identical to the MLE calculated for a *homogeneous* medium. (Propagation through a homogeneous medium is the special case of propagation through a random medium with zero fluctuation strength.) Comparisons between the two estimation methods found that the performance of the beamforming method was considerably worse than that of the maximum likelihood method with use of the correct fluctuation strength. Their findings emphasize the necessity of correctly incorporating the effects of a random medium on the wavefront.

Wilson [2] used the same general approach to study the effects of atmospheric turbulence on the performance bounds of linear acoustic arrays. This analysis considered a single monochromatic plane-wave source propagating in atmospheric turbulence and a LOS propagation path. The CRLB of the azimuth was calculated with the assumption that the source and noise components of the received signal had a Gaussian distribution with zero mean. Gaussian, von Kármán, and Kolomogorov turbulence models were examined. It was found that the array's

port applies to the AOAs, which represent the orientation of the wavefront normal when the sound reaches the array. For propagation in the atmosphere, the average horizontal (azimuthal) AOA is usually very close to the AOB, thereby making acoustic arrays well suited to determining the horizontal position of a source. The situation is usually quite different for the vertical (zenith) AOA, however. In this case, atmospheric refraction interferes with the ability to determine the AOB from the AOA by bending sound waves upward or downward. Because of refraction, most existing acoustic systems do not attempt to determine the zenith of a near-ground source.

performance degraded with increasing propagation distance, increasing frequency, and increasing turbulence strength.

By assuming that the signal of interest was zero-mean Gaussian, both Song and Ritcey [1] and Wilson [2] implicitly treated the case of waves *strongly scattered* by the turbulence. In strong scattering, the turbulence is sufficiently strong and/or the wavefronts propagate sufficiently far that the phase of the received signal is completely randomized. However, for most Army tactical scenarios involving acoustic ground sensors, the propagation distances are short enough that the signal is only *weakly scattered*, meaning that it has a deterministic mean component. This report generalizes the treatment of the previous authors by providing results valid for both strong and weak scattering.

The second main contribution of this report pertains to the problem of multiple unknowns in the FI. In Wilson [2], the FI was calculated assuming that the only unknown was the wavefront AOA. The source-receiver propagation distance and the turbulence parameters were implicitly assumed to be known. In a real scenario, this information may not be available. In this report we extend the analysis of Wilson [2]. The AOAs (azimuth and zenith), propagation distance, SNR, and turbulence parameters are treated as unknowns. The first and second moments of the scattered sound field are considered for a turbulent medium with fluctuations described by a von Kármán spectrum. Both a two-dimensional (2D) and a three-dimensional (3D) analysis are performed for a single monochromatic plane-wave source. A LOS propagation path is assumed. The primary interests of this report are to calculate the CRLBs of the AOAs and to observe how these bounds change with the introduction of additional unknown parameters. Therefore, we present only the CRLBs of the AOAs in this report and leave the discussion of the CRLBs of the other parameters for a later report because of the complexity of the results.

The signal processing theory is described in section 2 and the von Kármán turbulence model is described in section 3. The full theoretical model is derived in section 4. In sections 5 and 6, the CRLBs of the estimates are discussed for the cases of no turbulence and turbulence, respectively. Results are given in section 7 and conclusions are drawn in section 8. A table of symbols and abbreviations is given in appendix A.

2. Signal Processing Theory

2.1 Cramer-Rao Lower Bound

We wish to estimate a vector parameter $\mathbf{\Theta} = [\Theta_1\ \Theta_2\ \ldots\ \Theta_{\mathcal{N}}]^{\mathrm{T}}$. The minimum MSE of an unbiased estimator $\hat{\mathbf{\Theta}}$ about its actual value $\mathbf{\Theta}$ for a given algorithm may be calculated from the Cramer-Rao theorem [3,4], which gives

$$\left\langle\ (\Theta_\nu - \hat{\Theta}_\nu)^2\ \right\rangle \geq \left[\mathbf{J}^{-1}(\mathbf{\Theta})\right]_{\nu\nu}\ , \tag{1}$$

where $\mathbf{J}(\mathbf{\Theta})$ is the $\mathcal{N} \times \mathcal{N}$ FI matrix. (An estimator is said to be unbiased if and only if $\left\langle \hat{\mathbf{\Theta}} \right\rangle = \mathbf{\Theta}$.) The FI is related to the probability likelihood $\wp(\mathbf{x};\ \mathbf{\Theta})$ (the probability density function (PDF) of $\mathbf{x}$ with $\mathbf{\Theta}$ as a parameter) by

$$[\mathbf{J}(\mathbf{\Theta})]_{\lambda\nu} = -\left\langle\ \frac{\partial^2 \ln \wp(\mathbf{x};\ \mathbf{\Theta})}{\partial\Theta_\lambda \partial\Theta_\nu}\ \right\rangle, \tag{2}$$

where the expectation value is taken with respect to $\wp(\mathbf{x};\ \mathbf{\Theta})$ and the derivatives are evaluated at the true value of $\mathbf{\Theta}$. For some function $\boldsymbol{\xi}$, the estimator $\hat{\mathbf{\Theta}} = \boldsymbol{\xi}(\mathbf{x})$ can attain the CRLB if and only if [3]

$$\frac{\partial \ln \wp(\mathbf{x};\mathbf{\Theta})}{\partial \mathbf{\Theta}} = \mathbf{J}(\mathbf{\Theta})\left[\boldsymbol{\xi}\left(\mathbf{x}\right) - \mathbf{\Theta}\right]\ . \tag{3}$$

The likelihood function for real parameters of a complex Gaussian PDF with covariance matrix $\mathbf{C}_{\mathbf{x}}(\mathbf{\Theta})$ and mean $\boldsymbol{\mu}(\mathbf{\Theta})$ may be written [3]

$$\wp(\mathbf{x};\ \mathbf{\Theta}) = \frac{1}{\pi^{\mathcal{N}} \det\left[\mathbf{C}_{\mathbf{x}}(\mathbf{\Theta})\right]} \exp\left\{-\left[\mathbf{x} - \boldsymbol{\mu}(\mathbf{\Theta})\right]^{\dagger}\ \mathbf{C}_{\mathbf{x}}^{-1}(\mathbf{\Theta})\left[\mathbf{x} - \boldsymbol{\mu}(\mathbf{\Theta})\right]\right\}. \tag{4}$$

Its corresponding FI is

$$J_{\lambda\nu} = \mathrm{tr}\left(\mathbf{C}^{-1}\frac{\partial \mathbf{C}}{\partial\Theta_\lambda}\,\mathbf{C}^{-1}\,\frac{\partial \mathbf{C}}{\partial\Theta_\nu}\right) + 2\Re\left(\frac{\partial \boldsymbol{\mu}^{\dagger}}{\partial\Theta_\lambda}\,\mathbf{C}^{-1}\,\frac{\partial \boldsymbol{\mu}}{\partial\Theta_\nu}\right), \tag{5}$$

where the functional dependence has been dropped. If there are M independent and identically distributed data sets, the likelihood function is the product of M identical distribution functions, and hence the FI is M times the quanitity given in equation (5). Let there be n elements in the sensor array. Then $\mathbf{C}$ is an $n \times n$ matrix, and $\boldsymbol{\mu}$ is a column vector of length n. Let the subscripts $\lambda,\ \nu \in [1,\ \ldots,\ \mathcal{N}]$ be the indices on the parameters and $i,\ j \in [1,\ \ldots,\ n]$ be the indices for the elements of the sensor array.

Let us define $\sigma_\nu \equiv \sqrt{[\mathbf{J}^{-1}]_{\nu\nu}}$. (We may sometimes refer to the square root of the CRLB as SQRTCRLB.) The minimum value of σ_ν^2 is $\sigma_{\nu_0}^2 \equiv 1/J_{\nu\nu}$, i.e., the CRLB when Θ_ν is the only unknown. As the number of unknowns increases, σ_ν^2 will increase. This is readily seen by examining the FI for two unknowns. Suppose

$$\mathbf{J} = \begin{bmatrix} J_{11} & J_{12} \\ J_{21} & J_{22} \end{bmatrix} . \tag{6}$$

Then, as the FI is symmetric for real parameters,

$$\sigma_1^2 = \left(J_{11} - J_{12}^2/J_{22}\right)^{-1} . \tag{7}$$

Only if $J_{12} = 0$ do $\sigma_{1,2}^2 = \sigma_{1_0,2_0}^2$, and the estimates of Θ_1 and Θ_2 are said to be uncoupled. The quantity

$$\zeta = 1 - \frac{\sigma_{1_0}^2}{\sigma_1^2} = 1 - \frac{\sigma_{2_0}^2}{\sigma_2^2} = \frac{J_{12}^2}{J_{11}J_{22}} \tag{8}$$

provides a measure of the strength of the coupling between the estimates of Θ_1 and Θ_2: if $\zeta = 0$, the estimates are uncoupled; if $\zeta \ll 1$, the estimates of Θ_1 and Θ_2 are nominally coupled; and if $\zeta = 1$, there is not enough information to obtain an estimate of either Θ_1 or Θ_2 and the CRLB of each is infinite.

2.2 Signal Model

Consider an acoustic array with n sensors. We assume that the signal at each sensor results from: (1) the wave that has propagated from the source of interest, with φ and θ as the azimuthal and zenith AOAs, and (2) random noise. Let $\mathbf{p}(\varphi, \theta, t)$ and $\mathbf{N}(t)$ be the time-varying complex envelopes of the two contributions, respectively. These column vectors have n elements, one element corresponding to each sensor. The source contribution is time dependent because of the random turbulent effects. The noise, which is also time dependent, may result from wind noise or other competing acoustic sources. The total received signal is thus

$$\mathbf{s}(\varphi, \theta, t) = \mathbf{p}(\varphi, \theta, t) + \mathbf{N}(t) . \tag{9}$$

Let us assume that the source signal and the noise are uncorrelated. Then if the noise signals at the sensors are mutually uncorrelated and have an equal variance of σ_{N}^2, the total covariance is the sum

$$\mathbf{C} = \mathbf{C}_p + \mathbf{C}_{\mathrm{N}} = \mathbf{C}_p + \sigma_{\mathrm{N}}^2 \, \mathbf{I}_n , \tag{10}$$

where the subscript p refers to the pressure field of the sound wave of interest and N the noise. We assume that the noise has a Gaussian distribution with zero mean. Now by definition

$$[\mathbf{C}_p]_{ij} = \left\langle\ (p_i - \mu_i)(p_j - \mu_j)^*\ \right\rangle = \left\langle\ p_i\, p_j^*\ \right\rangle - \mu_i\, \mu_j^*\,, \quad \mu_i\ \equiv \left\langle\ p_i\ \right\rangle, \qquad (11)$$

where $\langle\cdot\rangle$ indicates the ensemble average. We take the values of $\left\langle\ p_i\, p_j^*\ \right\rangle$ and μ_i from results in the literature for acoustic wave propagation in a moving random medium as discussed in section 3.1.

3. Turbulence Model

Ideally, we should calculate the FI from the product of the probability likelihoods of the pressure field $\mathbf{p}$ and the noise $\mathbf{N}$. However, exact solutions for $\mathbf{p}$ do not exist (nor for $\wp(\mathbf{p})$), but solutions to the first and second moments do exist.

The rigorous solution for the pressure field associated with a sound wave propagating through a moving medium can be obtained as a closed set of fluid dynamic equations [5]. A pair of approximations are commonly applied to this equation set to make the problem tractable. The parabolic approximation, valid for small-angle propagation, provides reduction to a single equation. The Markov approximation, which assumes that the turbulence field has vanishing correlation in the propagation direction, subsequently allows the statistical moments of the sound-pressure field to be obtained in a closed form. These parabolic and Markov approximations are valid in the far field of the source, at observation points near the propagation axis ($\psi \ll 1$ where ψ is the angle off the propagation axis), and for $\mathcal{L} \gg \lambda > \ell$, where λ is the wavelength and $\mathcal{L}$ and ℓ are the outer (integral) and inner length scales of the turbulence, respectively. We use the solutions for the first and second moments of the sound pressure as given by Ostashev [5]. These results are outlined in the following section.

3.1 Solution for the First and Second Moments

Suppose that a sound wave is propagating along the x-axis. The parabolic and Markov approximations predict that the moments of the sound pressure will attenuate in a simple exponential manner. Defining the observation point as $\mathbf{r} = [x,\ y,\ z]$ and the acoustic wave number as $\mathbf{k}$, $|\mathbf{k}| = k = 2\pi/\lambda$, the equation for the first moment is then

$$\left\langle\ p(\mathbf{r})\ \right\rangle = e^{-\gamma x}\, p_{\mathrm{H}}\,(\mathbf{r})\ , \tag{12}$$

where γ is the extinction coefficient for the first moment and $p_{\mathrm{H}}(\mathbf{r})$ is the sound field in the absence of random inhomogeneities. For an incident plane wave, $p_{\mathrm{H}}(\mathbf{r}) = p_0\, e^{\mathrm{i}\mathbf{k}\cdot\mathbf{r}} = p_0\, e^{\mathrm{i}kx}$, where p_0 is a real-valued constant. We also define a saturation parameter Ω as

$$\Omega = 1 - e^{-2\gamma x}\,. \tag{13}$$

The first moment represents the unscattered (deterministic) part of the wave field. When $\gamma x \ll 1$, the saturation parameter is close to 0, scattering is small, and the signal at a single sensor exhibits little variability. When $\gamma x \gg 1$, $\Omega \approx 1$, and the scattered part of the field dominates.

We wish to know the second moment for two points near the x-axis, designated $\mathbf{r}_1 = [x,\ y_1,\ z_1]$ and $\mathbf{r}_2 = [x,\ y_2,\ z_2]$. For a fixed sensor separation, the second moment also undergoes an exponential diminishment:

$$\left\langle\, p\left(\mathbf{r}_1\right)\, p^*\left(\mathbf{r}_2\right)\,\right\rangle = p_{\text{II}}\left(\mathbf{r}_1\right)\, p^*_{\text{II}}\left(\mathbf{r}_2\right)\; e^{-\alpha(\rho)x}\,, \tag{14}$$

where $\boldsymbol{\rho} = \mathbf{r}_1 - \mathbf{r}_2$ is the sensor separation vector (transverse to the propagation direction) and α is the extinction coefficient for the second moment.

The extinction coefficients depend on the structure of the random medium. The result for the second moment is [5–8]

$$\alpha(\rho) = 2\pi k^2\,[f(0) - f(\rho)] \tag{15}$$

in which f is the two-dimensional (or projected) correlation function for the sound-speed fluctuations. The extinction coefficients for the first and second moments are related by

$$\gamma = \alpha(\infty)/2\,. \tag{16}$$

For most random media, including turbulence, $\alpha(\rho)$ initially increases monotonically with increasing ρ, but when ρ exceeds $\mathcal{L}$, $\alpha(\rho)$ asymptotically approaches a constant value [6]. Since $f(\rho) \to 0$ in the limit $\rho \to \infty$, this constant value is simply 2γ, given by

$$2\gamma = 2\pi k^2 f(0) = 2\varsigma^2 k^2 \mathcal{L}\,, \tag{17}$$

where ς^2 is the index-of-refraction variance. Hence the second moment will initially decrease with increasing ρ, but will eventually "saturate" at a fixed minimum value.

3.2 von Kármán Turbulence Model

Typical acoustic sensor arrays used by the Army have a sensor spacing larger than the height of the array from ground. As such, performance of these arrays is affected by the large eddies of the *energy-containing* (or *source*) subranges of the turbulence spectrum. This dependence on the large eddies distinguishes typical acoustical systems from optical ones,

whose performance depends primarily upon the smaller scale eddies in the *inertial* and *dissipation* subranges. In this report, we adopt the isotropic, homogeneous von Kármán turbulence model, since it is relatively simple and behaves fairly realistically in the energy-containing subrange. And, unlike the more commonly used Gaussian models, the von Kármán model accurately describes the inertial subrange of the turbulence spectrum.

The von Kármán form for the two-dimensional correlation function actually depends on whether the fluctuations in sound speed are induced by a scalar field (temperature or humidity) or a vector field (wind velocity). The functions for a scalar field f_s and a vector field f_v are [6]

$$f_s(\rho, \varsigma^2, l) = \frac{2\varsigma^2 l}{\sqrt{\pi}\,\Gamma\left(\frac{1}{3}\right)} \left(\frac{\rho}{2l}\right)^{\frac{5}{6}} K_{\frac{5}{6}}\left(\frac{\rho}{l}\right) \tag{18}$$

$$f_v(\rho, \varsigma^2, l) = \frac{2\varsigma^2 l}{\sqrt{\pi}\,\Gamma\left(\frac{1}{3}\right)} \left(\frac{\rho}{2l}\right)^{\frac{5}{6}} \left[K_{\frac{5}{6}}\left(\frac{\rho}{l}\right) - \frac{\rho}{2l} K_{\frac{1}{6}}\left(\frac{\rho}{l}\right)\right], \tag{19}$$

where l is a characteristic length scale (equal to $\Gamma(1/3)\,\Gamma^{-1}(5/6)\,\pi^{-1/2}\,\mathcal{L}$), $\Gamma(x)$ is the gamma function, and $K_\nu(x)$ is the modified Bessel function of order ν.

4. Full Theoretical Model

We now wish to apply the results presented in the previous sections to calculate the performance bounds of an acoustic sensor array operating in a turbulent medium with fluctuations described by a von Kármán spectrum. To do so, several approximations must be made. First, since a closed form expression for $\wp(\mathbf{p})$ does not exist in the solution to the parabolic equation, we make the approximation that $\wp(\mathbf{p})$ has a Gaussian distribution whose covariance matrix is described by the first and second moments of $\mathbf{p}$ as presented in the section 3.1. Second, the solution of the second moment given in section 3 is, strictly speaking, only valid in the far field for two observation points that have an equal distance parallel to the wavefront normal $\hat{\mathbf{n}}$ and have small components transverse to $\hat{\mathbf{n}}$. This is an unlikely scenerario, however, when one performs source localization with an acoustic array.

Let $\mathbf{r}$ be the vector from the center of the array normal to the plane of the source (parallel to $\hat{\mathbf{n}}$), so that r is the propagation distance of the wavefront to the center of the array. Let $\mathbf{r}'_i = [x'_i,\ y'_i,\ z'_i]$ be the vector from the center of the array to the ith sensor. We define $\mathbf{R}_i = \mathbf{r} + \mathbf{r}'_i$, so that $R_i^{\parallel}$ is the propagation distance of the wavefront to the ith sensor. Let $\boldsymbol{\rho}_{ij}$ be the separation between the ith and jth sensors, $\boldsymbol{\rho}_{ij} = \mathbf{R}_i - \mathbf{R}_j = \mathbf{r}'_i - \mathbf{r}'_j$, and let $\boldsymbol{\rho}_{ij}^{\perp}$ be the separation transverse to $\hat{\mathbf{n}}$. See figure 1. Strictly speaking equation (14) is valid only for $\boldsymbol{\rho}_{ij} = \boldsymbol{\rho}_{ij}^{\perp}$. However, we approximate

$$e^{-\alpha(\rho_{ij}^{\perp})r} \approx e^{-\alpha(\rho_{ij})r}\,. \tag{20}$$

We have two approximations here. First, we assume that the small angle approximation holds, so that $\rho_{ij}^{\perp} \approx \rho_{ij}$ and hence $\alpha(\rho_{ij}^{\perp}) \approx \alpha(\rho_{ij})$. Second, we take x in equation (14) to be $r = |\mathbf{r}|$. This is valid provided that for every i and j,

$$e^{-\alpha(\rho_{ij})r} \approx e^{-\alpha(\rho_{ij})R_i^{\parallel}} \approx e^{-\alpha(\rho_{ij})R_j^{\parallel}}\,. \tag{21}$$

Caution must be exercised when applying these approximations. For example, suppose that there are four sensors arranged in a rectangular configuration. If $\hat{\mathbf{n}}$ is in the plane of the sensor array, then there exist an i and j such that $\rho_{ij} \not\approx \rho_{ij}^{\perp}$. Whereas, if $\hat{\mathbf{n}}$ is nearly perpendicular to the array plane, for every i and j, $\rho_{ij} \approx \rho_{ij}^{\perp}$. See figure 2. Therefore, when

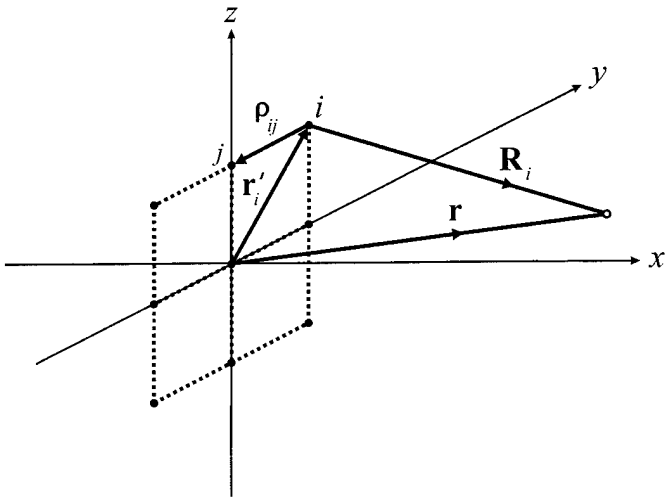

Figure 1. Coordinate system depicting vector from array center (origin) to ith sensor $\mathbf{r}'_i$, between ith and jth sensors $\boldsymbol{\rho}_{ij} = \mathbf{r}'_i - \mathbf{r}'_j$, from array center normal to source plane $\mathbf{r}$ (so that r is propagation distance to array center), and $\mathbf{R}_i = \mathbf{r} + \mathbf{r}'_i$. Closed circles represent sensors and open circle represents point at which $\mathbf{r}$ is normal to source plane.

considering problems strictly in two dimensions, we use a linear array. The use of other array geometries requires a different theoretical formulation than presented here. Similarly, when considering problems in three dimensions, we avoid the use of three-dimensional array configurations such cubes.

4.1 Covariance Matrix

Based on the assumptions just presented, we take the first and second moments to be

$$\mu_i = \tilde{\mu} e^{\mathrm{i}\phi_i} \tag{22}$$

$$\left\langle p_i p_j^* \right\rangle = p_0^2 e^{-\alpha(\rho_{ij})r} e^{\mathrm{i}\phi_{ij}}\,, \tag{23}$$

where

$$\tilde{\mu} = p_0 e^{-\gamma r} \tag{24}$$

$$\phi_i = \mathbf{k} \cdot \mathbf{R}_i + \chi \tag{25}$$

$$\phi_{ij} = \phi_i - \phi_j\,, \tag{26}$$

and where $\mathbf{r}$, $\mathbf{R}_i$, $\boldsymbol{\rho}_{ij}$, and p_0^2 are as previously defined*. The phase of the source χ is an unknown parameter and must be included in this treatment

*Note that we use the convention that μ_i is the ith component of the vector $\boldsymbol{\mu}$ (i.e., the value of the first moment of the sound field at the ith sensor) and is given by $\mu_i = \tilde{\mu} e^{\mathrm{i}\phi_i}$. In this manner, $|\mu_i| = \tilde{\mu}$ and $|\boldsymbol{\mu}| = \mu = \sqrt{n}\tilde{\mu}$.

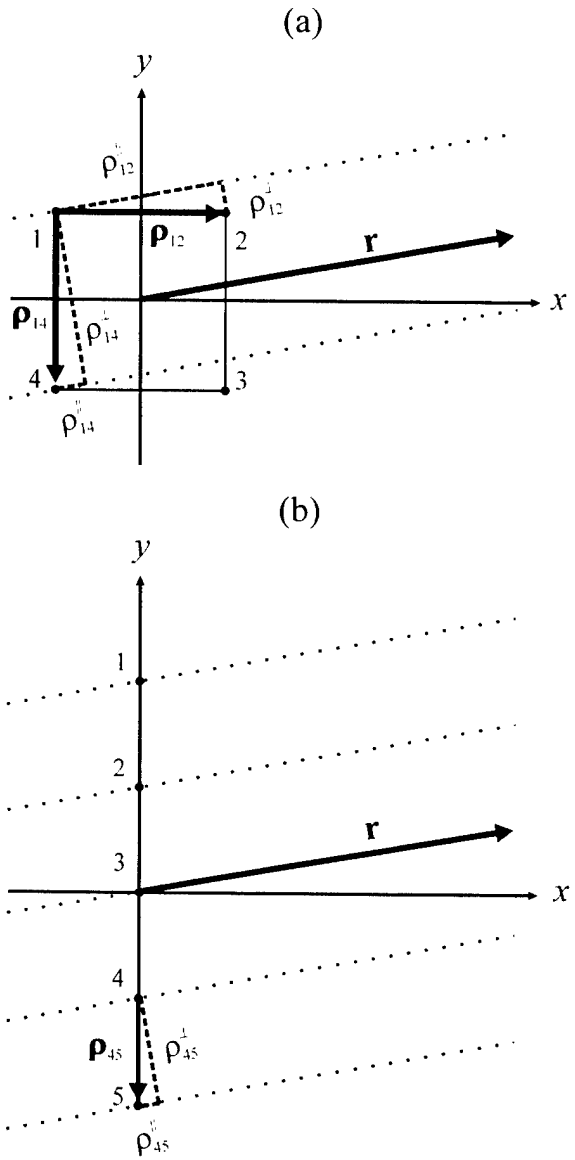

Figure 2. Array configurations in two dimensions. (a) Square array with sensors located at points 1–4. While $\rho_{14}^{\perp} \approx \rho_{14}$, $\rho_{12}^{\perp} \not\approx \rho_{12}$ and $\rho_{13}^{\perp} \not\approx \rho_{13}$. (b) Linear array. For every i and j, $\rho_{ij}^{\perp} \approx \rho_{ij}$.

(a) Two dimensions (b) Three dimensions

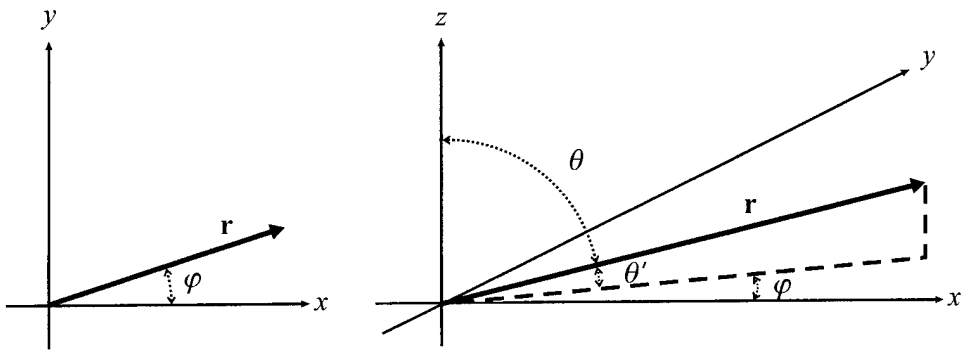

Figure 3. Coordinate system in (a) two dimensions and (b) three dimensions.

as we are assuming a nonzero mean. We thus write the elements of the total covariance matrix (equation (10)) as

$$C_{ii} = p_0^2 - \tilde{\mu}^2 + \sigma_{\mathrm{N}}^2 \tag{27}$$

$$C_{ij} = \left[p_0^2\, e^{-\alpha(\rho_{ij})\, r} - \tilde{\mu}^2\right] e^{\mathrm{i}\phi_{ij}}\ ,\ i \neq j\ . \tag{28}$$

Let us define

$$\mathbf{r} = r\ [\cos\varphi \sin\theta,\ \sin\varphi \sin\theta,\ \cos\theta] \tag{29}$$

$$\mathbf{r}_i' = \left[x_i',\ y_i',\ z_i'\right]\ , \tag{30}$$

so that φ is the azimuth, θ is the zenith (or declination), and $\theta' = \pi/2 - \theta$ is the elevation. See figure 3. Thus

$$\mathbf{k} \cdot \mathbf{R}_i = k\hat{\mathbf{r}} \cdot (\mathbf{r} + \mathbf{r}_i') = k\left(r + x_i' \cos\varphi \sin\theta + y_i' \sin\varphi \sin\theta + z_i' \cos\theta\right)\ . \tag{31}$$

The FI may now be readily calculated for those parameters we wish to consider as unknowns. While the derivatives of the covariance matrix and mean are straightforward, the derivatives with respect to the turbulence parameter l are tedious. For the interested reader, these are presented in appendices B and C.

4.2 Numerical Issues

Numerical difficulties may arise in trying to invert $\mathbf{J}$. Consider the diagonal terms of the FI matrix. The contributions from the propagation distance r and characteristic length scale l may differ by more than 10 orders of magnitude. This scale discrepancy may also occur for other

parameters. We construct a diagonal matrix $\mathbf{D}$ whose elements are the square root of the diagonal elements of the FI matrix, $D_{\lambda\nu} = J_{\lambda\lambda}^{-1/2}\delta_{\lambda\nu}$. The matrix $\mathbf{DJD}$ is now invertible. The CRLB of the unknown parameters may then be determined from

$$\left\langle \left(\Theta_\nu - \hat{\Theta}_\nu\right)^2 \right\rangle = \left[\mathbf{D}\left(\mathbf{DJD}\right)^{-1}\mathbf{D}\right]_{\nu\nu} . \tag{32}$$

The efficiency of the estimator is maintained by this process, as it is equivalent to a linear transformation of $\mathbf{\Theta}$. (Linear transformations preserve the efficiency of an estimator [3].)

5. Discussion: No Turbulence

We can gain insight into the estimation of the AOAs by first examining the limiting case of no turbulence. In the absence of turbulence, we simply have

$$\mathbf{C} = \sigma_{\mathrm{N}}^2 \mathbf{I}_n \quad \text{and} \quad \boldsymbol{\mu} = p_0 \left[e^{\mathrm{i}\phi_1} \; e^{\mathrm{i}\phi_2} \; \ldots \; e^{\mathrm{i}\phi_n} \right]^{\mathrm{T}} . \tag{33}$$

For parameters Θ_λ and Θ_ν of which σ_{N}^2 is independent, the Fisher information is determined from the second term in equation (5) and is given by

$$J_{\lambda\nu} = \frac{2M}{\sigma_{\mathrm{N}}^2} \frac{\partial \boldsymbol{\mu}^\dagger}{\partial \Theta_\lambda} \frac{\partial \boldsymbol{\mu}}{\partial \Theta_\nu} = 2M \frac{p_0^2}{\sigma_{\mathrm{N}}^2} \sum_{i=1}^{n} \frac{\partial \phi_i}{\partial \Theta_\lambda} \frac{\partial \phi_i}{\partial \Theta_\nu} . \tag{34}$$

5.1 Angle-of-Arrival Estimate in Two Dimensions

In two dimensions, $\phi_i = kr + kx_i' \cos\varphi + ky_i' \sin\varphi + \chi$. We assume r is known, if not, we can make the substitution $\chi \to \chi' \equiv kr + \chi$ below, and the results will still hold. We have

$$J_{\varphi\varphi} = 2M \frac{p_0^2}{\sigma_{\mathrm{N}}^2} \sum_{i=1}^{n} \left(\frac{\partial \phi_i}{\partial \varphi} \right)^2 = 2Mk^2 \frac{p_0^2}{\sigma_{\mathrm{N}}^2} \sum_{i=1}^{n} \left(-x_i' \sin\varphi + y_i' \cos\varphi \right)^2 \tag{35}$$

$$J_{\varphi\chi} = 2M \frac{p_0^2}{\sigma_{\mathrm{N}}^2} \sum_{i=1}^{n} \frac{\partial \phi_i}{\partial \varphi} \frac{\partial \phi_i}{\partial \chi} = 2Mk \frac{p_0^2}{\sigma_{\mathrm{N}}^2} \sum_{i=1}^{n} \left(-x_i' \sin\varphi + y_i' \cos\varphi \right) \tag{36}$$

$$J_{\chi\chi} = 2M \frac{p_0^2}{\sigma_{\mathrm{N}}^2} \sum_{i=1}^{n} \left(\frac{\partial \phi_i}{\partial \chi} \right)^2 = 2Mn \frac{p_0^2}{\sigma_{\mathrm{N}}^2} . \tag{37}$$

The estimates of φ and χ will decouple when $J_{\varphi\chi} = 0 \Rightarrow \sum x_i' = \sum y_i' = 0$, i.e., if the origin is taken to be at the center of the array.

Note that none of the elements of the FI is dependent upon the value of χ. This is expected as it is the arbitrary phase of the source, and its dependence should eventually cancel. Close inspection of the second term of equation (5) reveals that its dependence in the FI should cancel regardless of whether we consider turbulence or not.

5.2 Inclusion of χ for Non-Zero Mean Case

It was noted earlier that, as we are considering the case with a non-zero mean, the phase of the source χ in equation (25) must be included. The reason is most readily seen by examining the no turbulence case. For simplicity let us consider a line array along the y-axis and let us make no assumptions about the choice of the coordinate system. First suppose that $\phi_i = kr + ky_i' \sin\varphi$ where φ is unknown and r is known. Then

$$J_{\varphi\varphi} = 2M\frac{p_0^2}{\sigma_{\mathrm{N}}^2}\sum_{i=1}^{n}\left(\frac{\partial\phi_i}{\partial\varphi}\right)^2 = 2Mk^2\cos^2\varphi\frac{p_0^2}{\sigma_{\mathrm{N}}^2}\sum_{i=1}^{n}y_i'^2\,. \tag{38}$$

As $\sigma_\varphi^2 = 1/J_{\varphi\varphi}$, we see that we could choose a coordinate frame infinitely far away from the sensor array so that the CRLB of φ is zero.

As this is illogical, let us now suppose that $\phi_i = kr + ky_i' \sin\varphi + \chi$ where both φ and χ are unknown and r is known. The CRLB of φ is now

$$\begin{aligned}\sigma_\varphi^2 &= \left(J_{\varphi\varphi} - \frac{J_{\varphi\chi}^2}{J_{\chi\chi}}\right)^{-1} = \frac{\sigma_{\mathrm{N}}^2}{p_0^2}\left\{2Mk^2\cos^2\varphi\left[\sum_{i=1}^{n}y_i'^2 - \frac{1}{n}\left(\sum_{i=1}^{n}y_i'\right)^2\right]\right\}^{-1} \\ &= \frac{\sigma_{\mathrm{N}}^2}{p_0^2}\left[\frac{Mk^2\cos^2\varphi}{n}\sum_{i,j}\left(y_i' - y_j'\right)^2\right]^{-1}\,. \end{aligned}\tag{39}$$

Now σ_φ^2 is only dependent upon the separation of the sensors, regardless of the choice of coordinate system.

Second, let us consider that $\phi_i = kr + ky_i' \sin\varphi$ where r and φ are both unknown. Then $J_{\varphi\varphi}$ is given by equation (38) above and

$$J_{rr} = 2M\frac{p_0^2}{\sigma_{\mathrm{N}}^2}\sum_{i=1}^{n}\left(\frac{\partial\phi_i}{\partial r}\right)^2 = 2Mnk^2\frac{p_0^2}{\sigma_{\mathrm{N}}^2} \tag{40}$$

$$J_{r\varphi} = 2M\frac{p_0^2}{\sigma_{\mathrm{N}}^2}\sum_{i=1}^{n}\frac{\partial\phi_i}{\partial r}\frac{\partial\phi_i}{\partial\varphi} = 2Mk^2\cos\varphi\frac{p_0^2}{\sigma_{\mathrm{N}}^2}\sum_{i=1}^{n}y_i'\,. \tag{41}$$

Let us choose the origin to be at the center of the array so that the estimates of r and φ are uncoupled. Then $\sigma_r^2 = \left(2Mnk^2p_0^2/\sigma_{\mathrm{N}}^2\right)^{-1}$, i.e., we have the implausible result that the propagation distance can be determined to within the noise-to-signal ratio (NSR) for a plane wave with a single sensor array. Clearly, this bound could never be attained in practice.

Let us thus suppose that $\phi_i = kr + ky_i' \sin\varphi + \chi$ where r, φ, and χ are all unknown. Again let us chose the origin to be at the array center, so that

the estimate of φ is uncoupled from the estimates of r and χ. The FI matrix is then block diagonal, and the CRLBs of r and χ can be determined from the submatrix

$$\mathbf{J} = 2Mn\frac{p_0^2}{\sigma_{\mathrm{N}}^2}\begin{bmatrix} k^2 & k \\ k & 1 \end{bmatrix}, \tag{42}$$

where here J_{12} corresponds to $J_{r\chi}$. Because this matrix is singular, we have the expected result that the propagation distance and phase cannot be determined simultaneously for a plane wave.

Clearly from both examples presented, the phase angle χ must be included in ϕ_i for the non-zero mean case.

5.3 Angle-of-Arrival Estimates in Three Dimensions

Now let us consider the CRLB of the azimuth and zenith in three dimensions. (We note that we may interchangeably refer to the CRLB of the zenith (θ) and elevation (θ'), for as they are related by a linear transformation, their CRLBs are the same.) Suppose that $\phi_i = kr + kx_i' \cos\varphi \sin\theta + ky_i' \sin\varphi \sin\theta + kz_i' \cos\theta + \chi$ where φ, θ, and χ are unknown and r is known. We have

$$J_{\varphi\varphi} = 2Mk^2 \sin^2\theta \frac{p_0^2}{\sigma_{\mathrm{N}}^2} \sum_{i=1}^{n} \left(-x_i' \sin\varphi + y_i' \cos\varphi\right)^2 \tag{43}$$

$$J_{\theta\theta} = 2Mk^2 \frac{p_0^2}{\sigma_{\mathrm{N}}^2} \sum_{i=1}^{n} \left(x_i' \cos\varphi \cos\theta + y_i' \sin\varphi \cos\theta - z_i' \sin\theta\right)^2 \tag{44}$$

$$J_{\chi\chi} = 2Mn\frac{p_0^2}{\sigma_{\mathrm{N}}^2} \tag{45}$$

$$J_{\varphi\theta} = 2Mk^2 \sin\theta \frac{p_0^2}{\sigma_{\mathrm{N}}^2} \sum_{i=1}^{n} \Big[\left(y_i'^2 - x_i'^2\right) \cos\varphi \sin\varphi \cos\theta + x_i' y_i' \left(\cos^2\varphi - \sin^2\varphi\right) \cos\theta + x_i' z_i' \sin\varphi \sin\theta - y_i' z_i' \cos\varphi \sin\theta \Big] \tag{46}$$

$$J_{\varphi\chi} = 2Mk \sin\theta \frac{p_0^2}{\sigma_{\mathrm{N}}^2} \sum_{i=1}^{n} \left(x_i' \sin\varphi + y_i' \cos\varphi\right) \tag{47}$$

$$J_{\theta\chi} = 2Mk \frac{p_0^2}{\sigma_{\mathrm{N}}^2} \sum_{i=1}^{n} \left(x_i' \cos\varphi \cos\theta + y_i' \sin\varphi \cos\theta - z_i' \sin\theta\right) . \tag{48}$$

(Again note that the FI is independent of the value of χ.) For the estimate

of χ to decouple from the estimates of φ and θ

$$\sum_{i=1}^{n} x_i' = \sum_{i=1}^{n} y_i' = \sum_{i=1}^{n} z_i' = 0\,, \tag{49}$$

and for the estimates of φ and θ to decouple from one another

$$\sum_{i=1}^{n} y_i'^2 = \sum_{i=1}^{n} x_i'^2 \quad \text{and} \quad \sum_{i=1}^{n} x_i' y_i' = \sum_{i=1}^{n} x_i' z_i' = \sum_{i=1}^{n} y_i' z_i' = 0\,. \tag{50}$$

Symmetric array configurations such as a circular array with sensors placed at equal angular intervals or a rectangular grid with sensors placed at the lattice points meet these requirements provided that the origin is taken to be at the center of the array and that the array is located in the xy-plane. (We should note that Nielsen [9] has performed a similar analysis for a multiple-frequency, far-field, sine wave signal imbedded in Gaussian noise. The conditions he found for the estimates of all the angles to decouple are the same as for the simple case presented here. Among the literature which examine array configurations that result in the decoupling of the angle estimates, [10–12] may be of interest to the reader.)

If conditions (49) and (50) are met, then

$$J_{\varphi\varphi} = 2Mk^2 \sin^2\theta \frac{p_0^2}{\sigma_{\mathrm{N}}^2} \sum_{i=1}^{n} x_i'^2 \tag{51}$$

$$J_{\theta\theta} = 2Mk^2 \frac{p_0^2}{\sigma_{\mathrm{N}}^2} \sum_{i=1}^{n} \left(x_i'^2 \cos^2\theta + z_i'^2 \sin^2\theta \right)\,. \tag{52}$$

Note that the CRLB of φ is singular at $\theta = 0$. Clearly this choice of coordinate system is beneficial for estimations of angles that are not near the z-axis. Recall when we introduded the turbulence model that, as we are using the small angle approximation, we are interested in angles near the propapation axis. We therefore will not be able to uncouple the estimates of the zenith and azimuth when considering turbulence, as we will have to choose the array plane to be either the xz- or yz-plane.

In the following sections when we consider the case with turbulence, we will take the array to be in the yz-plane and the wavefront to propagate near the x-axis. Let us therefore examine the case of no turbulence for this configuration. We assume that equation (49) holds, so that the estimates of φ and θ are uncoupled from the estimate of χ. Moreover, consider an array geometry such that

$$\sum_{i=1}^{n} y_i' z_i' = 0 \quad \text{and} \quad \sum_{i=1}^{n} y_i'^2 = \sum_{i=1}^{n} z_i'^2 \equiv Y'^2\,, \tag{53}$$

(a square grid is one example). Then

$$J_{\varphi\varphi} = 2Mk^2Y'^2\frac{p_0^2}{\sigma_{\mathrm{N}}^2}\sin^2\theta\cos^2\varphi \tag{54}$$

$$J_{\theta\theta} = 2Mk^2Y'^2\frac{p_0^2}{\sigma_{\mathrm{N}}^2}\left(\sin^2\varphi\cos^2\theta + \sin^2\theta\right) \tag{55}$$

$$J_{\varphi\theta} = 2Mk^2Y'^2\frac{p_0^2}{\sigma_{\mathrm{N}}^2}\cos\varphi\sin\varphi\cos\theta\sin\theta\,. \tag{56}$$

Note that the coupling between the estimates of φ and θ is only angularly dependent,

$$\zeta = \frac{J_{\varphi\theta}^2}{J_{\varphi\varphi}J_{\theta\theta}} = \frac{\sin^2\varphi\cos^2\theta}{\sin^2\theta + \sin^2\varphi\cos^2\theta}\,. \tag{57}$$

It follows that

$$\sigma_\theta^2 = \frac{\sigma_{\mathrm{N}}^2}{2Mk^2Y'^2p_0^2\sin^2\theta} \tag{58}$$

$$\sigma_\varphi^2 = \frac{\sigma_{\mathrm{N}}^2}{2Mk^2Y'^2p_0^2}\frac{\sin^2\theta + \sin^2\varphi\cos^2\theta}{\cos^2\varphi\sin^4\theta}\,. \tag{59}$$

While σ_θ^2 is only dependent upon θ, σ_φ^2 is dependent upon both φ and θ. As we are considering propagation near the x-axis, it is useful to write the results in terms of the elevation (θ') as opposed to the zenith (θ). In this manner, we may use the small angle approximation to the power series expansion in both φ and θ'. The coupling coefficient is

$$\zeta = \frac{\sin^2\varphi\sin^2\theta'}{\cos^2\theta' + \sin^2\varphi\sin^2\theta'} \tag{60}$$

$$\approx \varphi^2\theta'^2 - \frac{1}{3}\varphi^4\theta'^2 + \frac{2}{3}\varphi^2\theta'^4\,. \tag{61}$$

Note that for either $\varphi = 0$ or $\theta' = 0$, $\zeta = 0$ and the estimates of φ and θ' are uncoupled as expected. We also see that for small angles the coupling between the estimates of φ and θ' is weak. In fact, at $\varphi = \theta' = 15°$, $\zeta = 4.79 \times 10^{-3}$. The CRLBs of θ' and φ are

$$\sigma_{\theta'}^2 = \frac{\sigma_{\mathrm{N}}^2}{2Mk^2Y'^2p_0^2}\sec^2\theta' \tag{62}$$

$$\approx \frac{\sigma_{\mathrm{N}}^2}{2Mk^2Y'^2p_0^2}\left(1 + \theta'^2 + \frac{2}{3}\theta'^4 + \frac{17}{45}\theta'^6 + \ldots\right) \tag{63}$$

and

$$\sigma_\varphi^2 = \frac{\sigma_{\mathrm{N}}^2}{2Mk^2Y'^2p_0^2}\left(\sec^2\theta' + \sec^4\theta'\tan^2\varphi\right) \tag{64}$$

$$\approx \frac{\sigma_{\mathrm{N}}^2}{2Mk^2Y'^2p_0^2}\left(1 + \theta'^2 + \varphi^2 + \frac{2}{3}\theta'^4 + \frac{2}{3}\varphi^4 + 2\theta'^2\varphi^2 + \frac{17}{45}\theta'^6 + \frac{17}{45}\varphi^6 + \frac{7}{3}\varphi^2\theta'^4 + \frac{4}{3}\varphi^4\theta'^2 + \ldots\right). \tag{65}$$

Note that $\sigma_\varphi^2(\varphi,\theta') = \sigma_\varphi^2(\theta',\varphi)$ holds up to $4th$ order in the expansion; for $\varphi = \theta' = 15°$, there is a 0.13 percent difference between the exact expression and the $4th$-order approximation, and a 1.5 percent difference for the $2nd$-order approximation.

6. Discussion: Turbulence

6.1 Angle-of-Arrival Estimate in Two Dimensions

Let us consider the CRLB of the AOA φ in two dimensions when incorporating turbulence. In the presence of turbulence, we find (numerically) that choosing the origin to be at the center of the array is no longer a sufficient condition for the estimates of the azimuth and phase angle to decouple. In addition, we must have a symmetric array configuration such as a linear array with mirror symmetry about the origin, (note that the stronger condition of uniform spacing is not needed). The estimates of φ and χ will also be uncoupled for a set of parallel linear arrays with uniform sensor spacing, however, the condition for the small angle approximation, given in equation (20), is violated with this array geometry. The results are independent of the value of χ, as we noted earlier they should be.

In Wilson [2], the CRLB of the AOA was analysed in-depth for the two-dimensional case assuming a zero mean and a single unknown parameter φ. We now wish to examine the difference when the mean is incorporated. For simplicity, let us begin by examing a simple two-element array and considering the unknowns φ and χ. We assume that all other parameters are known. In appendix D, the FI for a two-point sensor array is derived. In deriving equations (D-1)–(D-7), no assumptions are made about the form of the derivatives of the covariance matrix or the mean vector. In deriving equations (D-8) and (D-9), it is assumed that $\partial a/\partial\Theta_\lambda = \partial\beta/\partial\Theta_\lambda = \partial\tilde{\mu}/\partial\Theta_\lambda = 0$, where $a = C_{11} = C_{22} = p_0^2 - \tilde{\mu}^2 + \sigma_N^2$ in equation (27) and $\beta = |C_{12}| = |C_{21}| = p_0^2 e^{-\alpha(\rho_{12})r} - \tilde{\mu}^2$ in equation (28). As noted before, the estimates of the two parameters Θ_λ and Θ_ν will be uncoupled if $J_{\lambda\nu} = 0$.

Suppose that $\Theta_\lambda = \varphi$ and $\Theta_\nu = \chi$. By substituting the derivatives presented in appendix B into equation (D-9), we find

$$J_{\varphi\chi} = \frac{2M^2\tilde{\mu}^2}{a+\beta}\left(\frac{\partial\phi_1}{\partial\varphi} + \frac{\partial\phi_2}{\partial\varphi}\right) = \frac{2M^2\tilde{\mu}^2 k\left[-(x_1' + x_2')\sin\varphi + (y_1' + y_2')\cos\varphi\right]}{a+\beta}. \tag{66}$$

Therefore, the estimates of φ and χ will be uncoupled provided $x_1' = -x_2'$ and $y_1' = -y_2'$. Let $x_1' = x_2' = 0$ and $y_1' = -y_2' = d/2$. Then the CRLB of φ is $1/J_{\varphi\varphi}$, which from equation (D-8) , is

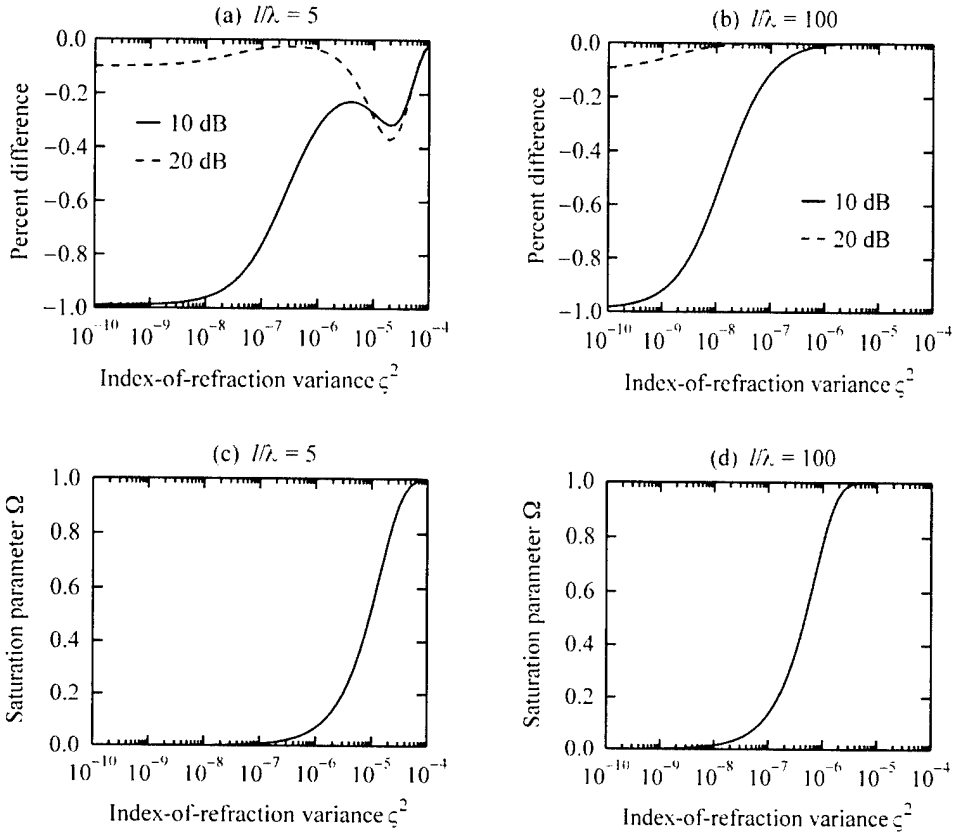

Figure 4. Percent difference of σ_φ calculated with a nonzero mean and with a zero mean versus ς^2 is in (a) and (b) for different values of l/λ. Corresponding saturation parameter is in lower figures (c) and (d). Calculations are in 2D for $\varphi = 0\,, r/\lambda = 250\,, d/\lambda = 0.5\,, n = 5,$ and a scalar von Kármán spectrum.

$$\sigma_\varphi^2 = \frac{a^2 - \beta^2}{Mk^2d^2\cos^2\varphi\left[2\beta^2 + \tilde{\mu}^2\left(a + \beta\right)\right]} \tag{67}$$

$$= \frac{p_0^4\left[1 - e^{-2\alpha(d)r}\right] - 2p_0^2\tilde{\mu}^2\left[1 - e^{-\alpha(d)r}\right] + \sigma_{\mathrm{N}}^2\left(2p_0^2 - 2\tilde{\mu}^2 + \sigma_{\mathrm{N}}^2\right)}{Mk^2d^2\cos^2\varphi\left\{2p_0^4e^{-2\alpha(d)r} + p_0^2\tilde{\mu}^2\left[1 - 3e^{-\alpha(d)r}\right] + \tilde{\mu}^2\sigma_{\mathrm{N}}^2\right\}}\,. \tag{68}$$

For $\tilde{\mu} = 0$ we recover the result presented in Wilson [2]. Whether or not the mean is incorporated, when $\varphi = 0$, the source is broadside to the sensors, and the performance is maximal. When $\varphi = \pi/2$, the source is in line with the sensors, and the solution is singular. Even though $\varphi = \pi/2$ is not consistent with the small angle approximation, the solution should be singular at $\varphi = \pi/2$.

In figures 4 to 6 the percent difference between σ_φ with and without the

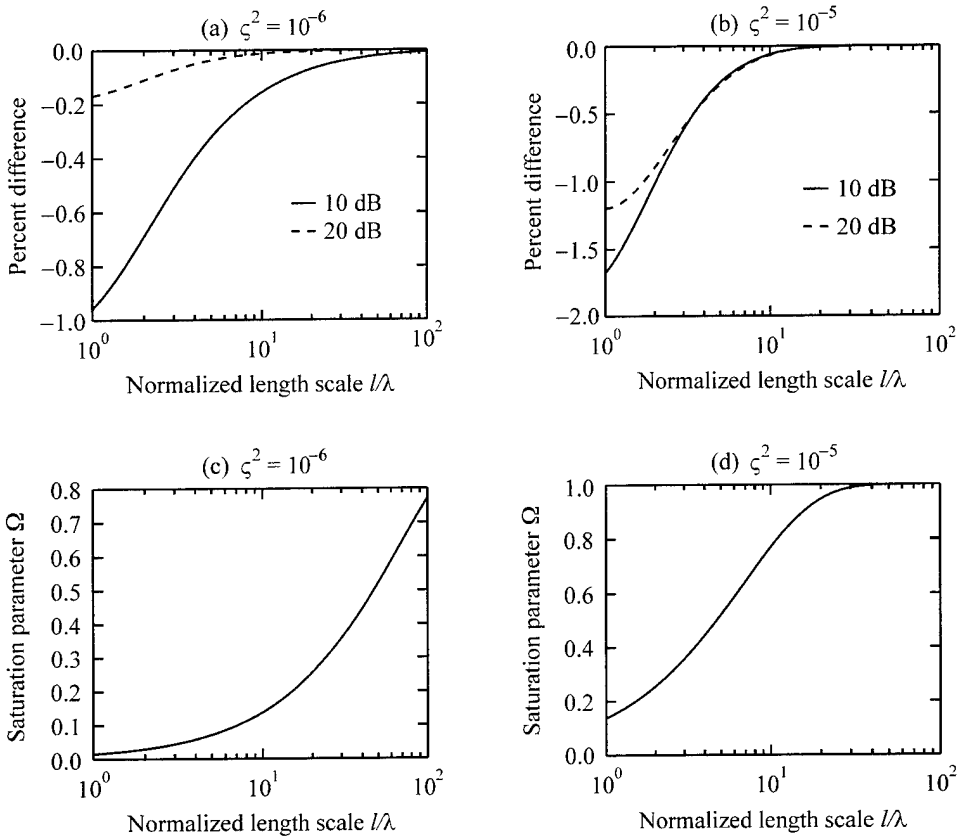

Figure 5. Percent difference of σ_φ calculated with a nonzero mean and with a zero mean versus l/λ is in (a) and (b) for different values of ς^2. Corresponding saturation parameter is in lower figures (c) and (d). Calculations are in 2D for $\varphi = 0$, $r/\lambda = 250$, $d/\lambda = 0.5$, $n = 5$, and a scalar von Kármán spectrum.

mean term is presented using a scalar von Kármán spectrum. A linear array with 5 sensors spaced in equal intervals of d is considered. The upper graphs (a) and (b) in figure 4 depict the percent difference versus the index-of-refraction variance ς^2 for fixed values of r/λ, l/λ, and d/λ and two values of the SNR. The lower graphs (c) and (d) give the corresponding saturation parameter Ω. In figures 5 and 6 the percent difference and saturation parameter are plotted versus l/λ and r/λ, respectively. (In presenting the results, it is more natural to use the normalized distances, as then the moments have no explicit wavelength dependence.) Notice that the percent difference goes to zero as the saturation parameter tends to one, as it must. Even for low saturation, the percent difference is still small. The results are similar for a vector von Kármán spectrum.

We also find, numerically, that the estimate of φ is uncoupled from the

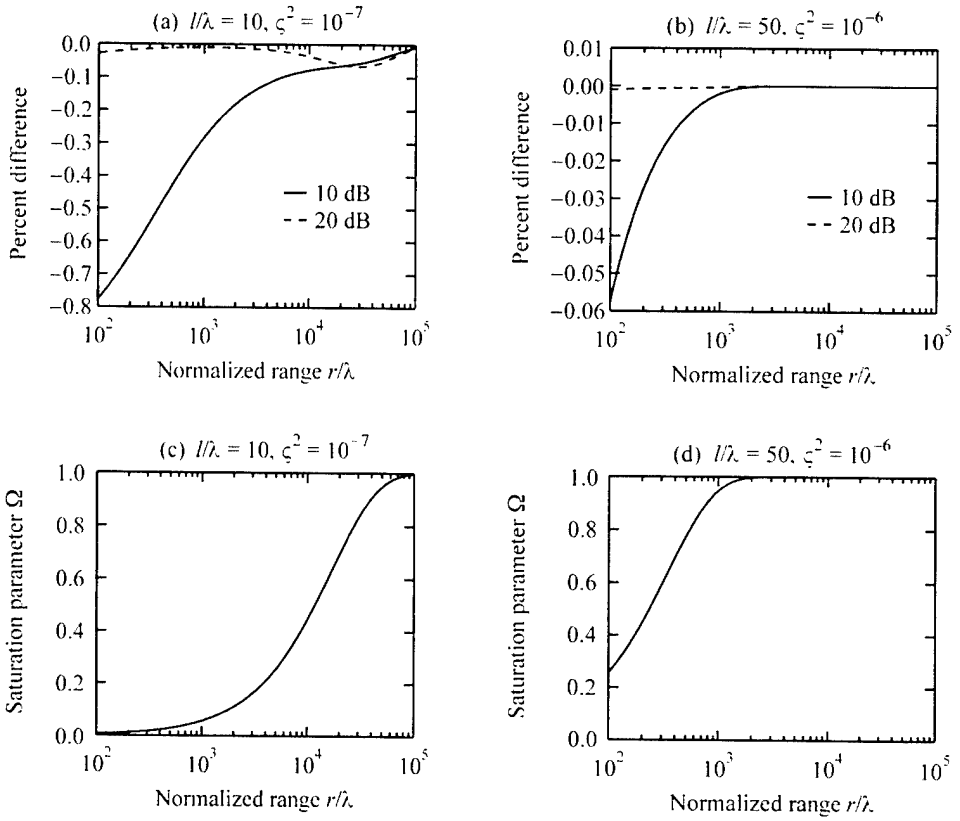

Figure 6. Percent difference of σ_φ calculated with a nonzero mean and with a zero mean versus r/λ is in (a) and (b) for different values of l/λ and ς^2. Corresponding saturation parameter is in lower figures (c) and (d). Calculations are in 2D for $\varphi = 0$, $d/\lambda = 0.5$, $n = 5$, and a scalar von Kármán spectrum.

estimates of all the other parameters: r, l, ς^2, and SNR (or NSR). The estimates of φ and r will decouple provided that the origin is taken at the center of the array and that the array is symmetric; again a linear array with mirror symmetry about the origin is sufficient. There are no conditions for the estimate of φ to decouple from the estimates of the remaining parameters. If we consider a simple two-element array, we can readily see why this occurs.

Suppose that $\Theta_\lambda = \varphi$. Inspection of equation (D-9) reveals that the estimate of φ will decouple from the estimate of any parameter of which ϕ_i is independent. Therefore, as ϕ_i is independent of l, ς^2, and SNR, the estimates of these parameters decouple from the estimate of φ. For $\Theta_\nu = r$, we have

$$J_{\varphi r} = \frac{2M^2\tilde{\mu}^2 k}{a+\beta}\left(\frac{\partial\phi_1}{\partial\varphi} + \frac{\partial\phi_2}{\partial\varphi}\right) = \frac{2M^2\tilde{\mu}^2 k^2}{a+\beta}\left[-\left(x_1' + x_2'\right)\sin\varphi + \left(y_1' + y_2'\right)\cos\varphi\right] . \qquad (69)$$

Therefore, the estimates of r and φ will decouple provided $x_1' = -x_2'$ and $y_1' = -y_2'$.

6.2 Angle-of-Arrival Estimates in Three Dimensions

As we wish to meet the conditions of the small-angle approximation, we take the yz-plane to be the array plane and the x-axis to be near the propagation axis. As noted earlier, the estimates of θ and φ will be coupled for this choice. As with the two-dimensional case, we find (numerically) that for the estimates of θ and φ to decouple from the estimates of r and χ, we must take the origin to be at the array center and use a symmetric array configuration such as a rectangular grid with mirror symmetry in y and z about the origin. The estimates of θ and φ are found (numerically) to decouple from the estimates of all the remaining parameters. The results are independent of the value of χ.

7. Results

7.1 Two-Dimensional Analysis

It was shown in section 6.1 that the percent difference in the CRLB of φ when using a non-zero mean versus a zero mean is small. While the CRLB of φ was examined in detail in Wilson [2], we present the results here, nonetheless, as we are using a modified version of the 2D correlation functions f_s and f_v. The results presented are for a linear array with 5 sensors spaced in equal intervals of d. The origin is taken to be the array center so that the estimate of φ decouples from the estimates of all other parameters. As the CRLB for M independent and identically distributed datasets is $1/\sqrt{M}$ times the CRLB for one dataset, all results are presented for $M = 1$.

The CRLB of φ for $\varphi = 0$ is plotted versus ς^2 and l/λ in figures 7 and 8 for SNRs of 10 and 20 dB, respectively, and for fixed values of the other

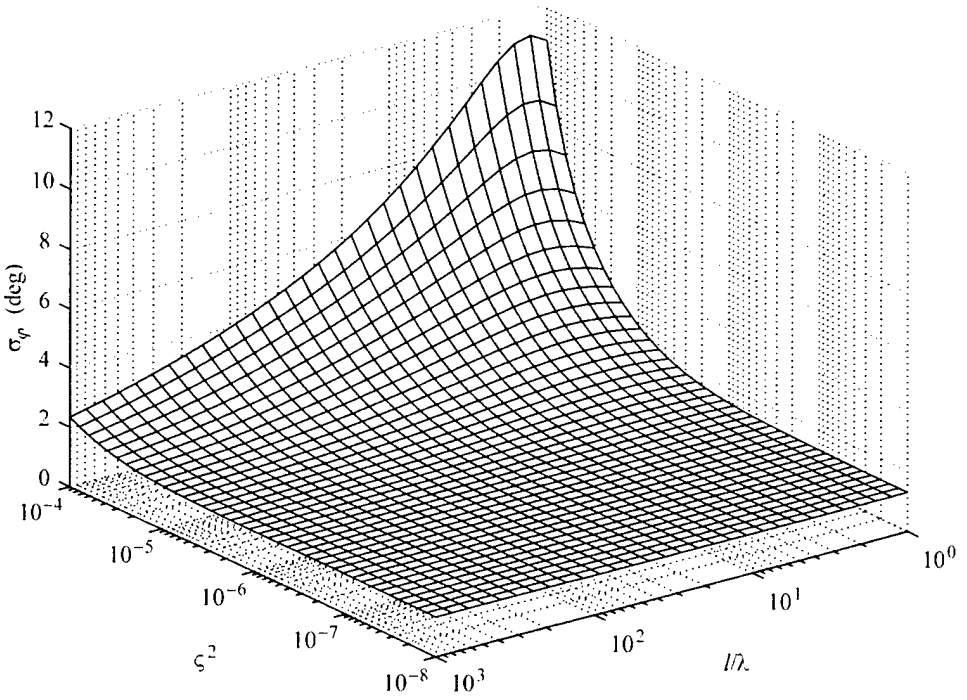

Figure 7. 2D analysis of σ_φ versus ς^2 and l/λ for $\varphi = 0$, $r/\lambda = 500$, $d/\lambda = 0.5$, $n = 5$, SNR = 10 dB, and a scalar von Kármán spectrum.

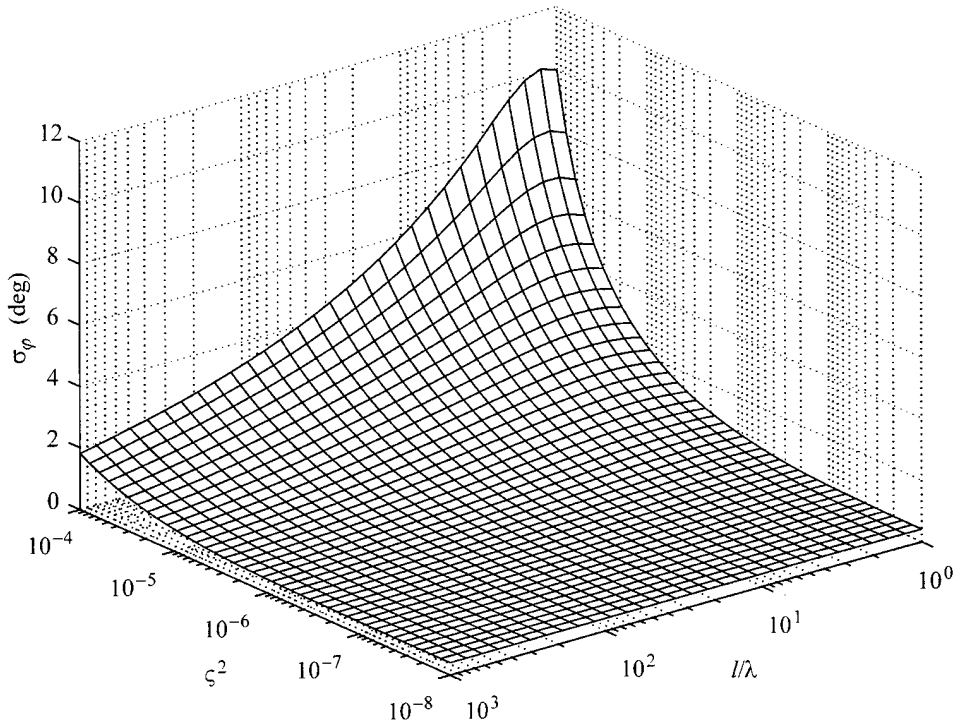

Figure 8. 2D analysis of σ_φ versus ς^2 and l/λ for $\varphi = 0$, $r/\lambda = 500$, $d/\lambda = 0.5$, $n = 5$, SNR = 20 dB, and a scalar von Kármán spectrum.

parameters. A scalar von Kármán spectrum is used. A peak is evident in σ_φ at the larger values of ς^2 and smaller values of l/λ. In this region both $\exp[-\alpha(\rho_{ij})r]$ and $\exp(-2\gamma r)$ are small. In fact, in the limit that $\exp[-\alpha(\rho_{ij})r]$ and $\exp(-2\gamma r)$ simultaneously approach zero, $\sigma_\varphi^2 \to \infty$ as $\mathbf{C} \to \sigma_N^2 \mathbf{I}_n$ and $\boldsymbol{\mu} \to 0$. For small values of ς^2 and of l/λ, both $\exp[-\alpha(\rho_{ij})r]$ and $\exp(-2\gamma r)$ are approaching the maximum value of 1.0, and hence σ_φ^2 is approaching the limit of $\left(k^2 d^2 \cos^2\varphi\, p_0^2/\sigma_N^2\right)^{-1}$ for no turbulence. The value of σ_φ increases with decreasing SNR.

In figures 9 and 10, σ_φ for $\varphi = 0$ is plotted versus d/λ and ς^2 again for two values of the SNR, fixed values of all the other parameters, and a scalar von Kármán spectrum. In figure 11, σ_φ for $\varphi = 0$ is plotted versus d/λ and r/λ. For all cases, the peak in σ_φ occurs when both $\exp[-\alpha(\rho_{ij})r]$ and $\exp(-2\gamma r)$ are small.

In figure 12 we examine σ_φ at $\varphi = 0$ as a function of the normalized propagation distance r/λ for a couple of values each of the SNR, ς^2, and l/λ. For $\varsigma^2 = 10^{-6}$, the performance degrades with increasing r/λ, especially for $r/\lambda \gtrsim 10^4$. However, for $\varsigma^2 = 10^{-4}$, the performance degrades almost exponentially for $r/\lambda \gtrsim 10^3$ when $l/\lambda = 100$ and for

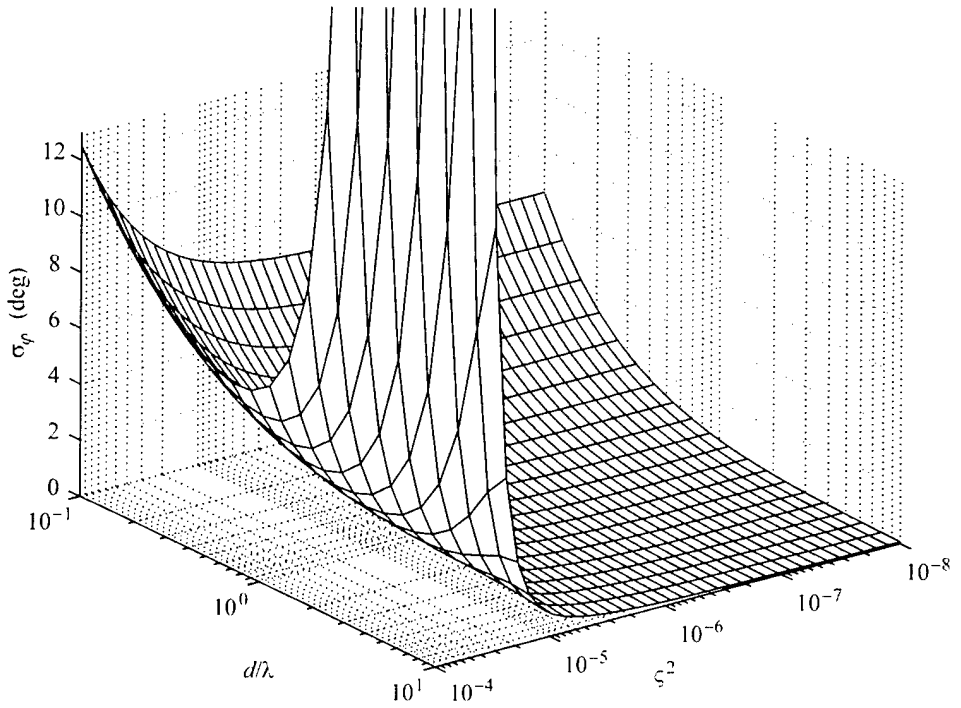

Figure 9. 2D analysis of σ_φ versus d/λ and ς^2 for $\varphi = 0$, $r/\lambda = 500$, $l/\lambda = 10$, $n = 5$, SNR = 10 dB, and a scalar von Kármán spectrum.

$r/\lambda \gtrsim 10^2$ when $l/\lambda = 10$. Intuitively, we expect that for regions of high turbulence the best accuracy will be attained for short propagation distances.

The CRLB of φ for other values of φ has the same behavior as for $\varphi = 0$, with σ_φ increasing slightly. In figure 13, σ_φ is plotted versus φ for two values of each r/λ, l/λ, ς^2, and SNR. A scalar von Kármán turbulence spectrum is used. We see that for $\varsigma^2 = 10^{-6}$ depicted in the upper graph (a), σ_φ is most sensitive to the SNR; whereas, for $\varsigma^2 = 10^{-4}$ depicted in (b), σ_φ is more sensitive to changes in the normalized length scale.

The results for a vector von Kármán spectrum are similar to those of the scalar spectrum: the shapes are nearly identical, but the value of σ_φ is for the most part larger. In figures 14 and 15 the ratio $\sigma_\varphi^v/\sigma_\varphi^s$ is plotted versus l/λ and ς^2 for SNRs of 10 and 20 dB, respectively. The superscripts v and s respectively refer to a vector and scalar spectrum. Note that the largest difference occurs when $\exp[-\alpha_v(\rho_{ij})r]$ is appreciably smaller than $\exp[-\alpha_s(\rho_{ij})r]$.

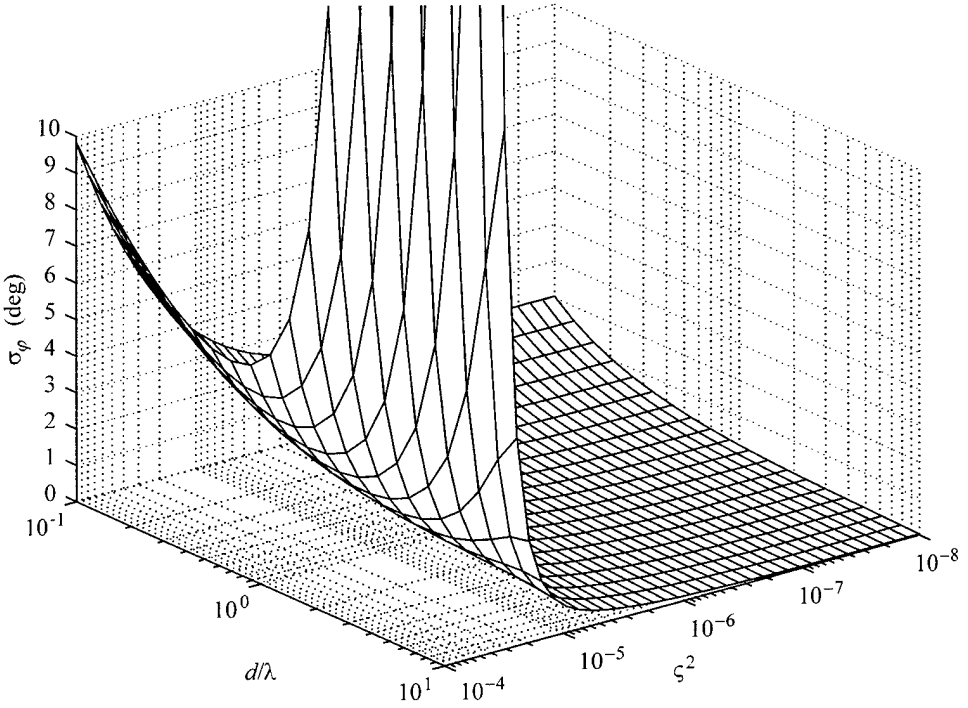

Figure 10. 2D analysis of σ_φ versus d/λ and ς^2 for $\varphi = 0$, $r/\lambda = 500$, $l/\lambda = 10$, $n = 5$, SNR = 20 dB, and a scalar von Kármán spectrum.

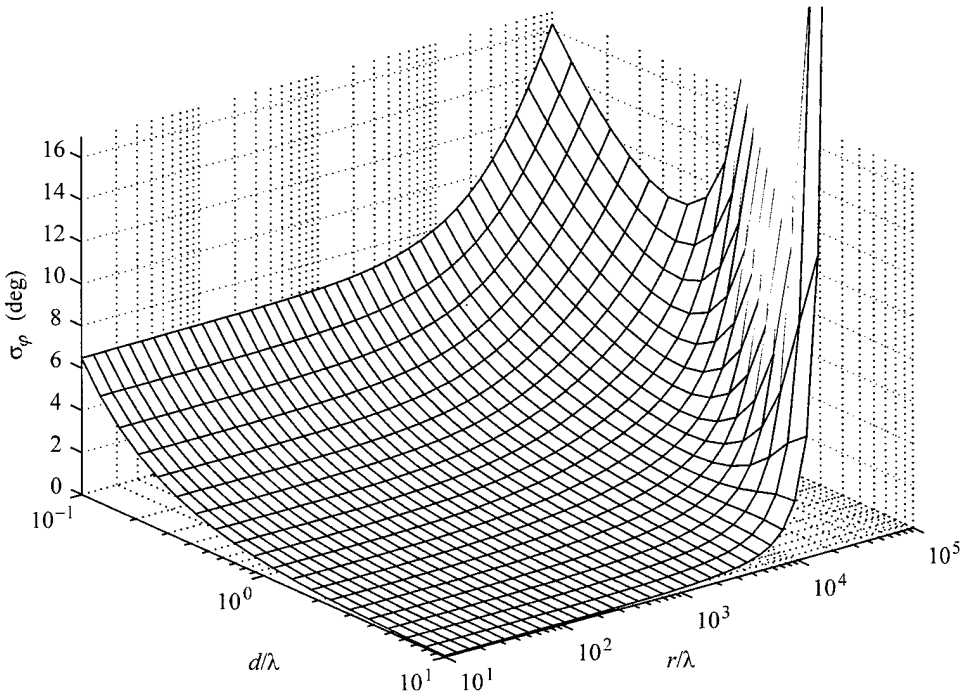

Figure 11. 2D analysis of σ_φ versus d/λ and r/λ for $\varphi = 0$, $\varsigma^2 = 10^{-6}$, $l/\lambda = 10$, $n = 5$, SNR = 10 dB, and a scalar von Kármán spectrum.

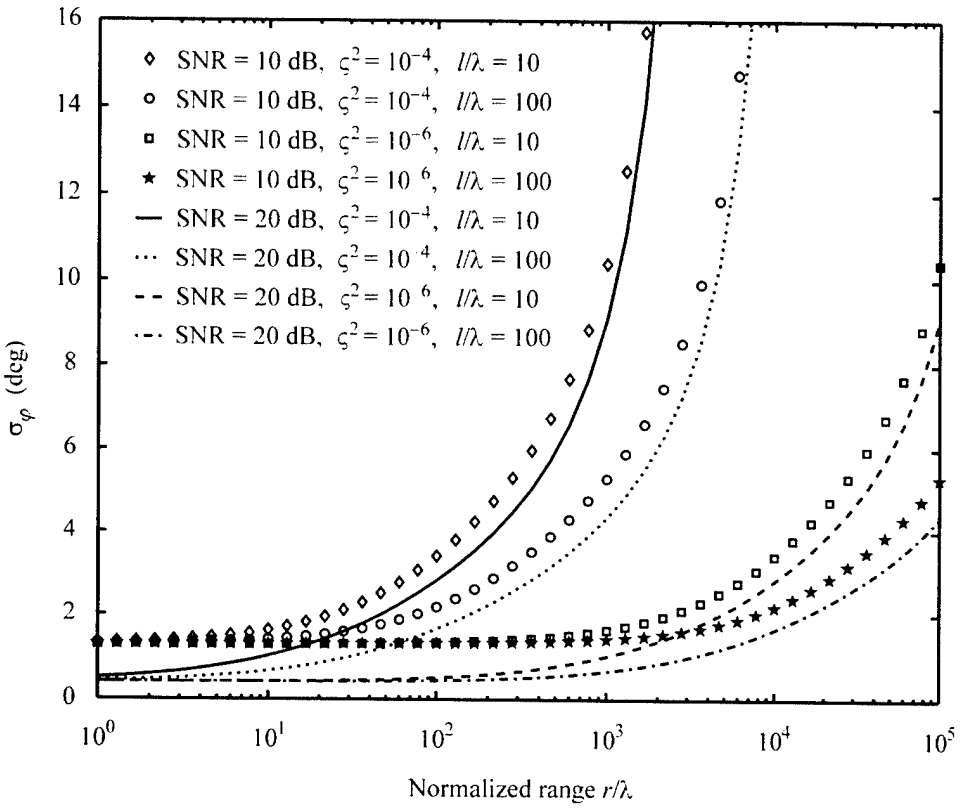

Figure 12. 2D analysis of σ_φ versus r/λ for different values of SNR, ς^2, and l/λ. All curves are for at $\varphi = 0$, $d/\lambda = 0.5$, $n = 5$, and a scalar von Kármán spectrum.

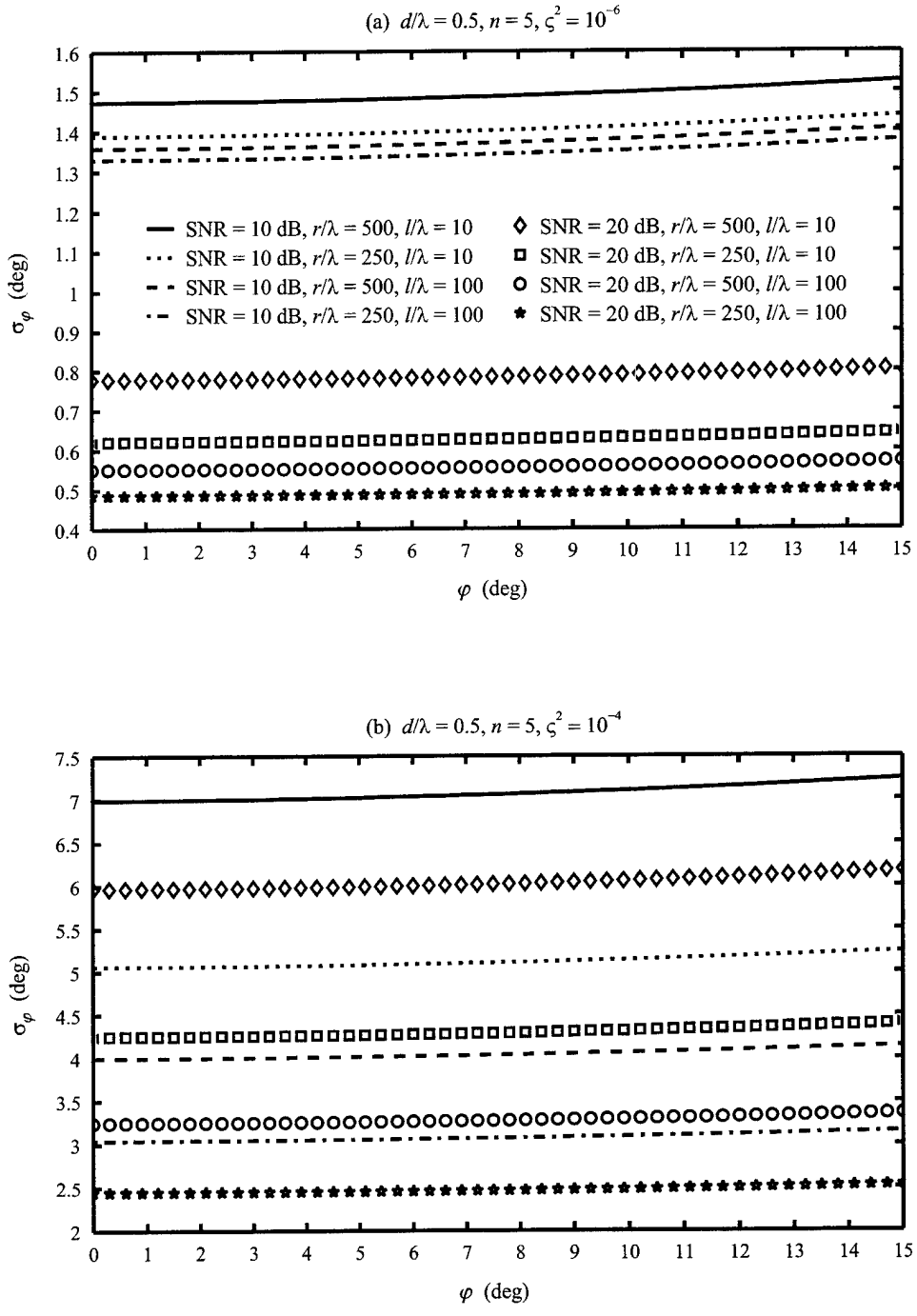

Figure 13. 2D analysis of σ_φ versus φ. A scalar von Kármán spectrum is used.

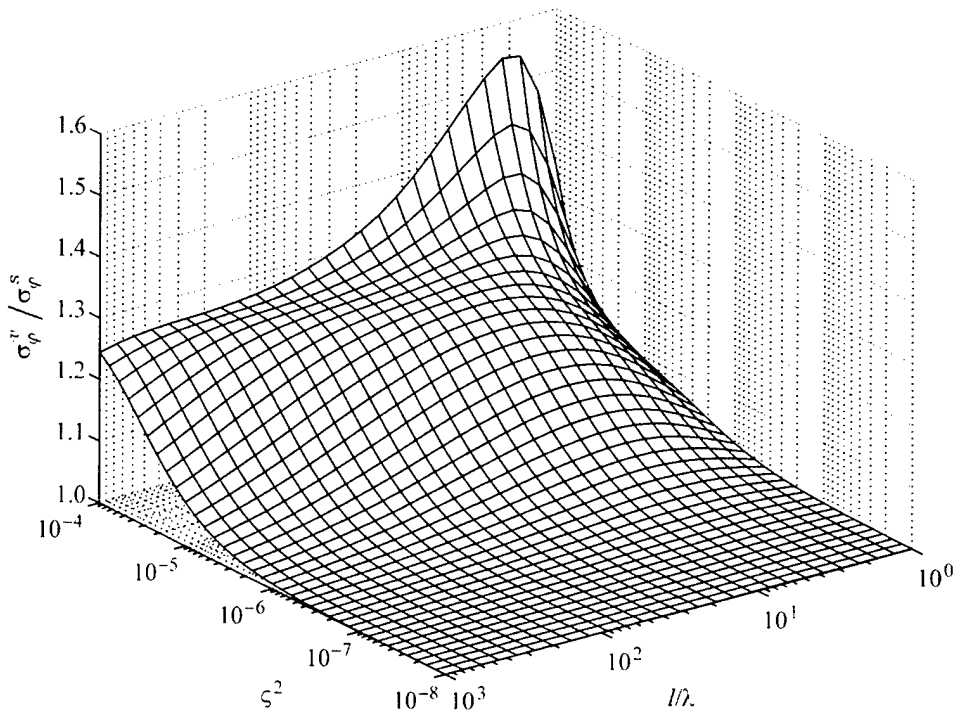

Figure 14. 2D analysis of ratio $\sigma_\varphi^v/\sigma_\varphi^s$ versus l/λ and ς^2 for $\varphi = 0$, $r/\lambda = 500$, $d/\lambda = 0.5$, $n = 5$, and SNR = 10 dB.

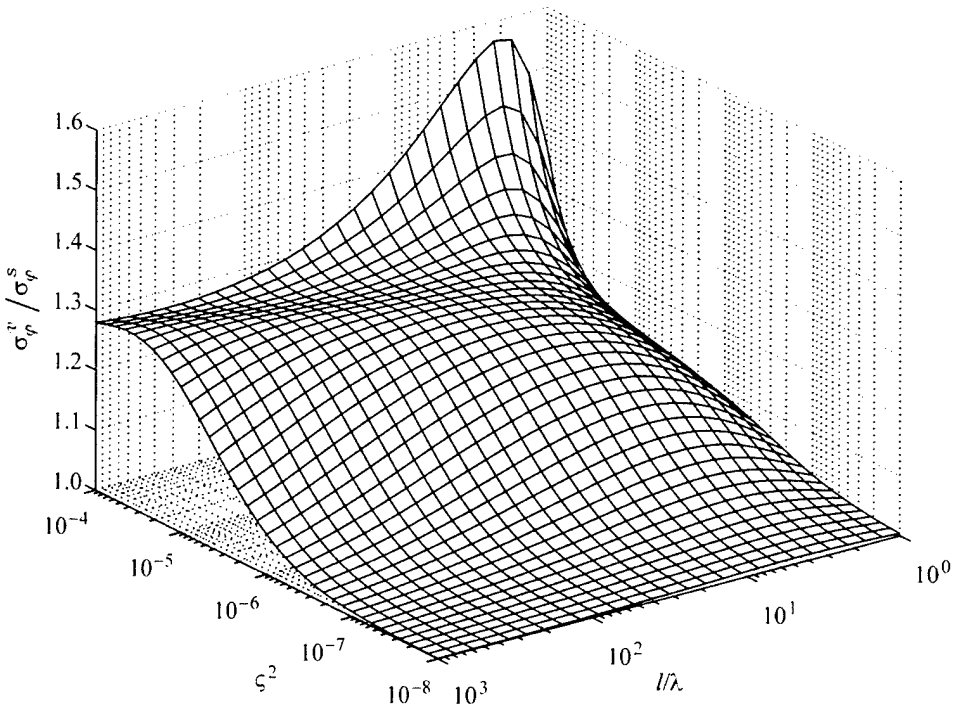

Figure 15. 2D analysis of ratio $\sigma_\varphi^v/\sigma_\varphi^s$ versus l/λ and ς^2 for $\varphi = 0$, $r/\lambda = 500$, $d/\lambda = 0.5$, $n = 5$, and SNR = 20 dB.

7.2 Three-Dimensional Analysis

We choose the x-axis to be the near-propagation axis and take the sensor array to be in the yz-plane. As noted earlier, this will result in the coupling of the estimates of φ and θ. The array geometry considered for this analysis is a 4×4 square grid with spacing of d. The origin is taken to be the array center. In this way, the estimates of φ and θ will decouple from the estimates of r and χ, as well as the estimates of the other parameters. Again all results presented are for $M = 1$.

The values of σ_φ, σ_θ, σ_{φ_0}, and σ_{θ_0} are the same at $\varphi = 0$ and $\theta = \pi/2$ due to symmetry. In figures 16 and 17, σ_φ at $\varphi = 0$ and $\theta = \pi/2$ is plotted versus l/λ and ς^2 for SNRs of 10 and 20 dB, respectively, and fixed values of the other parameters. A scalar von Kármán turbulence spectrum is used. We see the same behavior as for the two-dimensional case. The peak in σ_φ corresponds to the region where both $\exp[-\alpha(\rho_{ij})r]$ and $\exp(-2\gamma r)$ are small. The shape is similar to that in 2D, but the overall values are smaller, especially for large values of ς^2 and small values of l/λ. This is expected as a 4×4 array in 3D should provide more "information" than a 5-point

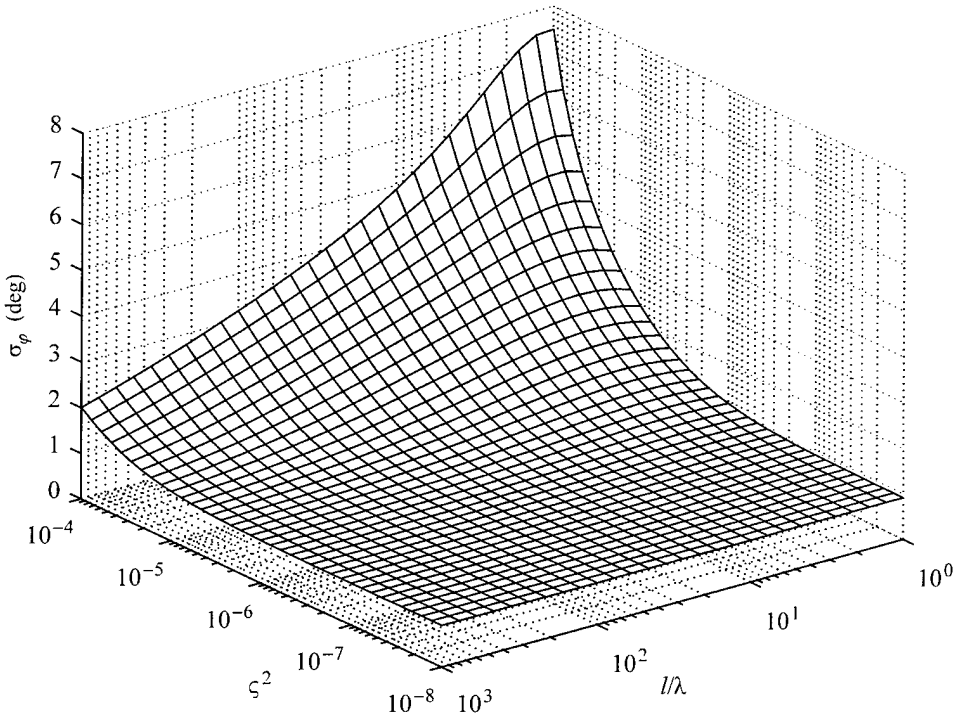

Figure 16. 3D analysis of σ_φ versus l/λ and ς^2 for $\varphi = 0$, $\theta = \pi/2$, $r/\lambda = 500$, $d/\lambda = 0.5$, $n_y = n_z = 4$, SNR $= 10$ dB, and a scalar von Kármán spectrum. At $\varphi = 0$ and $\theta = \pi/2$, $\sigma_\varphi = \sigma_\theta = \sigma_{\varphi 0} = \sigma_{\theta 0}$.

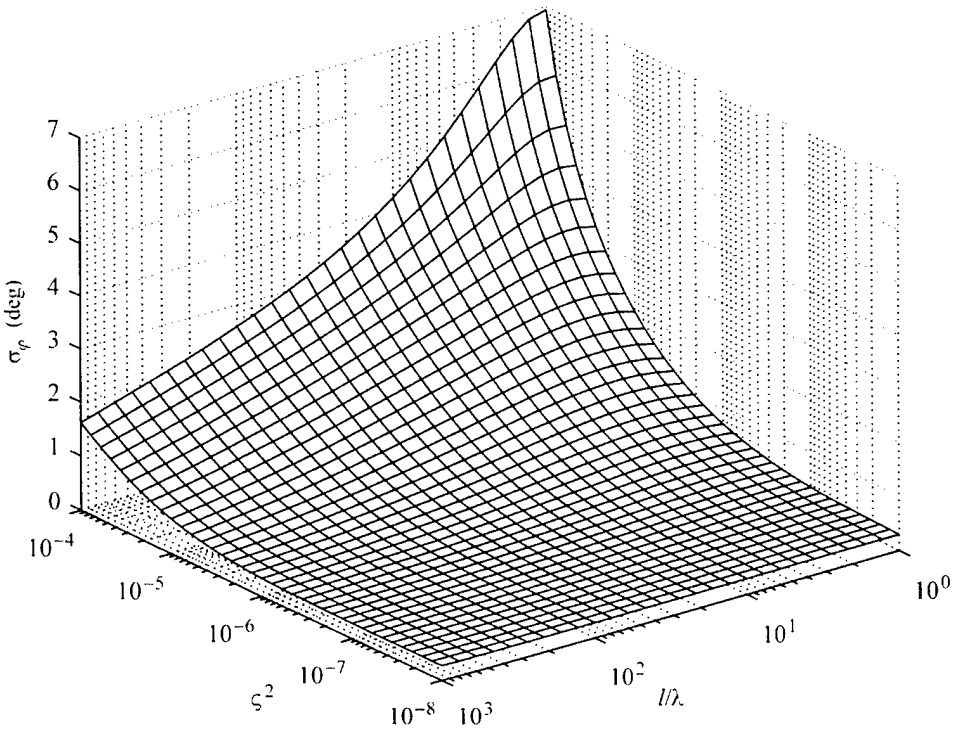

Figure 17. 3D analysis of σ_φ versus l/λ and ς^2 for $\varphi = 0$, $\theta = \pi/2$, $r/\lambda = 500$, $d/\lambda = 0.5$, $n_y = n_z = 4$, SNR = 20 dB, and a scalar von Kármán spectrum.

linear array in 2D. The behavior for other values of φ and θ is similar.

In figure 18 we examine σ_φ at $\varphi = 0$ and $\theta = \pi/2$ as a function of the normalized propagation distance r/λ for a couple of values each of the SNR, ς^2, and l/λ. As with the 2D case, we see that the performance degrades most rapidly with increasing r/λ for $\varsigma^2 = 10^{-4}$; for the 3D case, however, the near exponential rise in σ_φ now occurs at slightly larger values of r/λ.

As in the 2D case, the behavior of σ_φ and σ_θ for a vector von Kármán spectrum is similar to that of a scalar von Kármán spectrum: the CRLBs for the vector spectrum increase most significantly over those for the scalar spectrum in regions where $\exp[-\alpha_v(\rho_{ij})r]$ is appreciably smaller than $\exp[-\alpha_s(\rho_{ij})r]$. The ratio $\sigma_\varphi^v/\sigma_\varphi^s$ at $\varphi = 0$ and $\theta = \pi/2$ is plotted versus l/λ and ς^2 for SNRs of 10 and 20 dB in figures 19 and 20, respectively.

Figure 21 examines σ_φ and $\sigma_{\theta'}$ as functions of φ and θ', as well as the coupling between the estimates of φ and θ', for $\varsigma^2 = 10^{-6}$ and $l/\lambda = 10$. A scalar von Kármán spectrum is used. From figure 21(a), a contour graph of σ_φ for θ' versus φ, we see that for small angles $\sigma_\varphi(\varphi, \theta') = \sigma_\varphi(\theta', \varphi)$. This symmetry was also seen for small angles in the no-turbulence case.

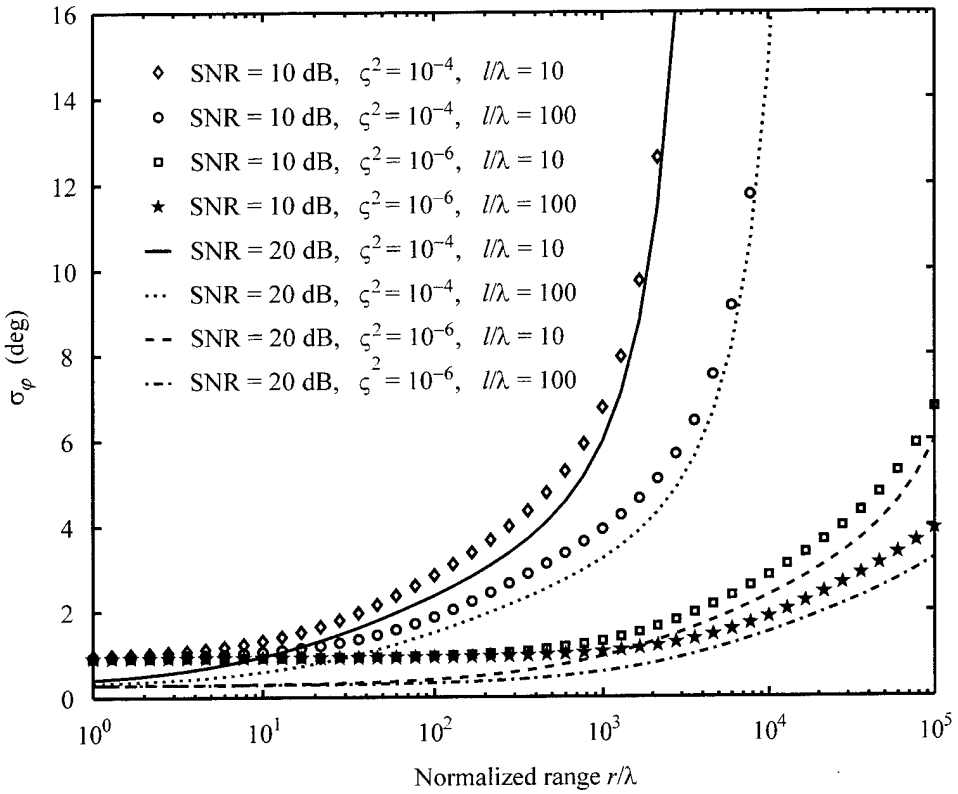

Figure 18. 3D analysis of σ_φ versus r/λ for $\varphi = 0$, $\theta = \pi/2$, $d/\lambda = 0.5$, $n_y = n_z = 4$, and a scalar von Kármán spectrum.

Figure 21(b) gives σ_φ as a function of φ for fixed values of θ'. Now, $\sigma_{\theta'}$, on the other hand, is dependent upon θ' but is independent of φ, as indicated in figure 21(c). Again this is the same behavior as in the no-turbulence case. As the estimate of neither φ nor θ' is coupled to the estimate of any other parameter, we may use equation (8) to gauge how strong the coupling between the estimates of φ and θ' is. We first note that σ_{φ_0} and $\sigma_{\theta'_0}$ are both dependent upon φ and θ'. In figure 21(d), ζ is plotted versus φ for fixed values of θ'. We see that the coupling is in fact weak. In figure 22(a-d) the same is presented but for $\varsigma^2 = 10^{-4}$ and $l/\lambda = 10$. Figures 21(d) and 22(d) appear identical. In fact we find, to within the numerical accuracy of this calculation, that ζ is the same as for the no turbulence case (see equations (57) and (60)), regardless of the the value of r/λ, d/λ, SNR, l/λ, or ς^2, and regardless of the von Kármán spectrum used.

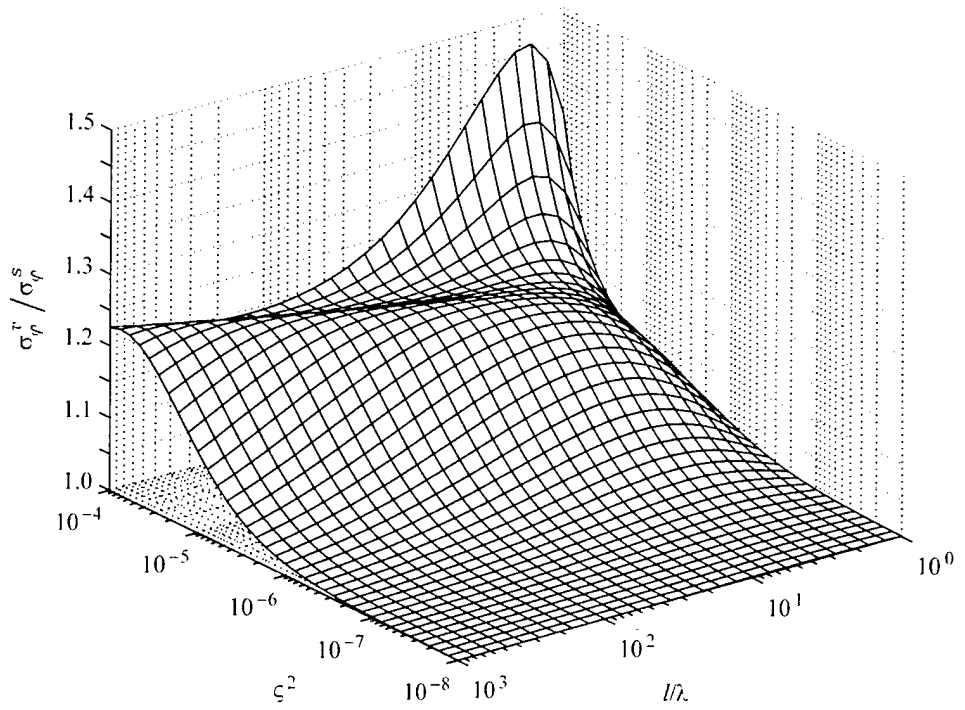

Figure 19. 3D analysis of ratio $\sigma_\varphi^v/\sigma_\varphi^s$ versus l/λ and ς^2 for $\varphi = 0$, $\theta = \pi/2$, $r/\lambda = 500$, $d/\lambda = 0.5$, $n_y = n_z = 4$, and SNR = 10 dB.

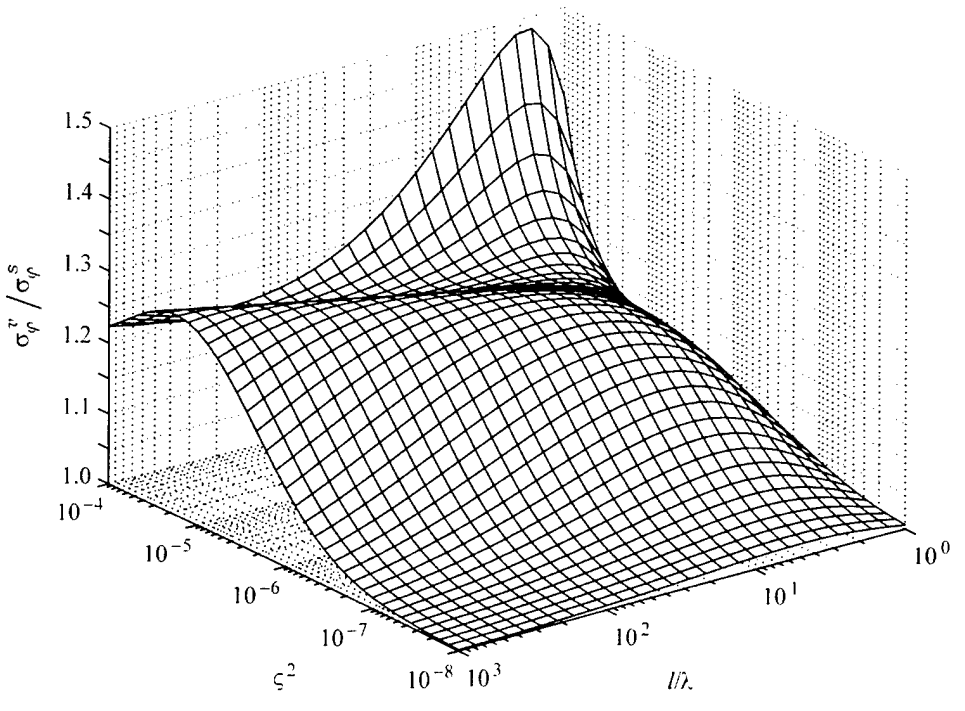

Figure 20. 3D analysis of ratio $\sigma_\varphi^v/\sigma_\varphi^s$ versus l/λ and ς^2 for $\varphi = 0$, $\theta = \pi/2$, $r/\lambda = 500$, $d/\lambda = 0.5$, $n_y = n_z = 4$, and SNR = 20 dB.

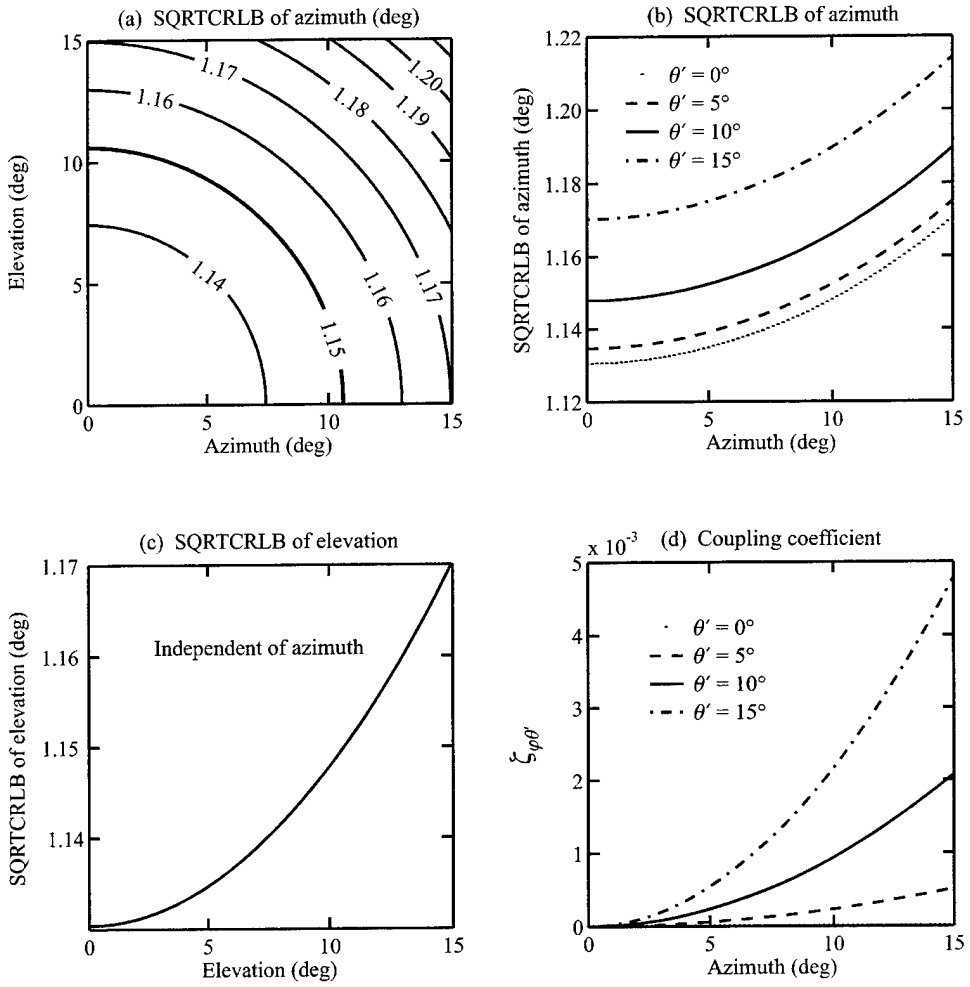

Figure 21. (a) Contour of σ_φ for θ' versus φ. (b) Plot of σ_φ versus φ for fixed θ'. (c) Plot of $\sigma_{\theta'}$ versus θ'. (d) Plot of ζ versus φ for fixed θ'. All curves are for $r/\lambda = 500$, $l/\lambda = 10$, $\varsigma^2 = 10^{-6}$, $d/\lambda = 0.5$, $n_y = n_z = 4$, SNR = 10 dB, and a scalar von Kármán spectrum.

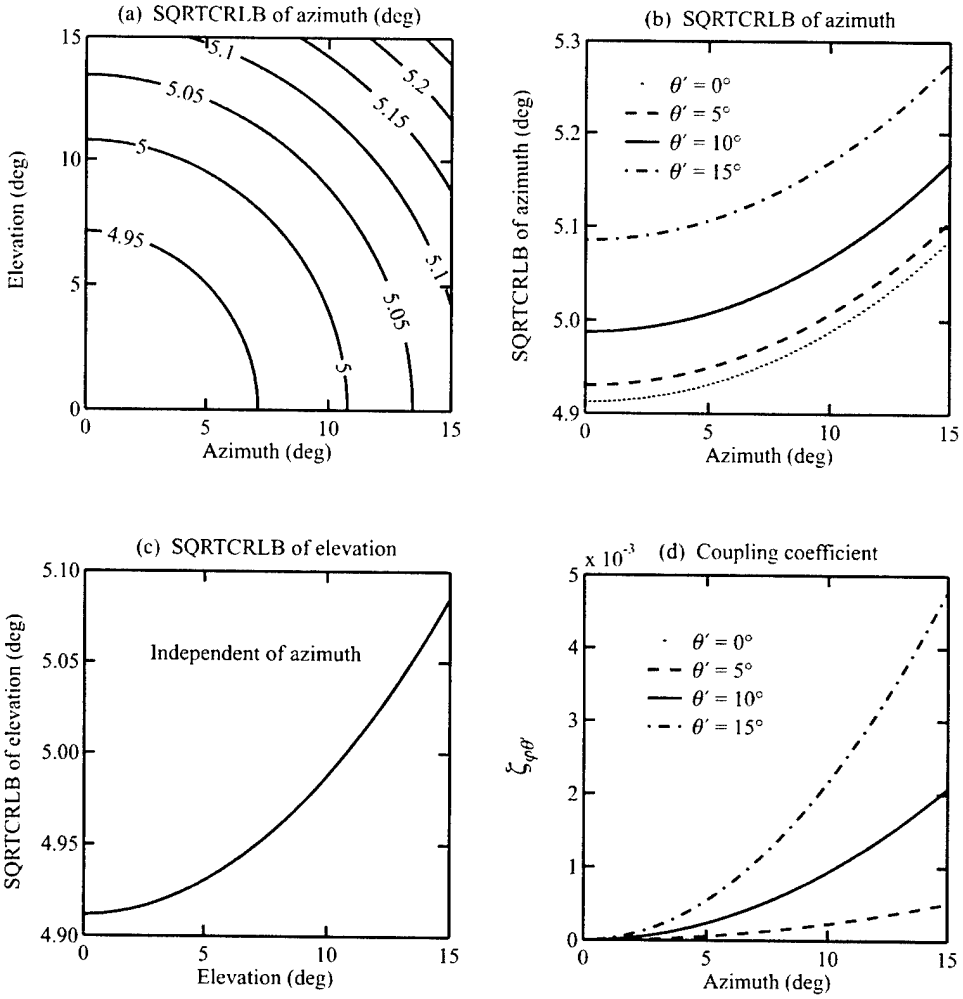

Figure 22. (a) Contour of σ_φ for θ' versus φ. (b) Plot of σ_φ versus φ for fixed θ'. (c) Plot of $\sigma_{\theta'}$ versus θ'. (d) Plot of ζ versus φ for fixed θ'. All curves are for $r/\lambda = 500$, $l/\lambda = 10$, $\varsigma^2 = 10^{-4}$, $d/\lambda = 0.5$, $n_y = n_z = 4$, SNR = 10 dB, and a scalar von Kármán spectrum.

7.3 Cramer-Rao Lower Bound of Other Parameters

Though we have not examined the CRLB of the other parameters in this report, a brief comment is in order. For large values of the index-of-refraction variance and small values of the normalized length scale, we find that for $\Theta \in [l/\lambda,\ \varsigma^2,\ r/\lambda]$, σ_Θ/Θ may be less than one for a sufficient number M of independent and identically distributed datasets. However, for other values of ς^2 and l/λ, $\sigma_\Theta/\Theta \gg 1$. Therefore, the regions in which σ_φ is strongly dependent upon Θ correspond to the regions in which σ_Θ/Θ is smallest; similarly the regions in which σ_φ is nearly independent of Θ, correspond to the regions in which Θ cannot be estimated from the model presented here. Due to the complexity of the analysis of σ_Θ, it is left for another date.

8. Summary and Conclusions

We have examined the performance bounds of acoustic arrays operating in atmospheric turbulence with fluctuations described by a von Kármán spectrum. The analysis featured three main improvements upon earlier work:

- The performance bounds were generalized to weak as well as strong scattering.
- Multiple unknowns, such as the propagation distance of the wavefront and the turbulence parameters, were incorporated.
- AOA estimates for three-dimensional problems (i.e., two bearing angles) were considered.

Our primary interest in this report was to analyze the CRLBs of the AOAs. For an incident plane wave, we have found that an appropriate choice of coordinate system and array geometry leads to the decoupling of the estimates of the AOAs from the estimates of the other parameters: the normalized propagation distance (r/λ), SNR, turbulence parameters (l/λ and ς^2), and phase angle (χ). In order to remain consistent with the small-angle approximation, we had to choose a coordinate system that resulted in the coupling of the estimates of the azimuth and zenith; the coupling, however, was small. We have found that the CRLBs of the AOAs increase significantly for large values of the normalized propagation distance and index-of-refraction variance. However, for small values of the index-of-refraction variance and normalized propagation distance, the SNR is the limiting factor.

The results in this report demonstrate that scattering by atmospheric turbulence significantly affects the performance of acoustic sensor arrays. Future efforts should attempt to incorporate the additional phenomena of ground reflections and refraction by atmospheric wind and temperature gradients. These phenomena will likely have considerable impact on the ability to estimate the elevation angle. However, numerical techniques will probably be required to model these complications.

Appendix A. Nomenclature

A.1 Symbols

$\mathbb{C}$	Complex
$*$	Complex conjugate
$\equiv$	Defined as
$\in$	Element of
$\langle \cdot \rangle$	Ensemble average or expectation value
$\dagger$	Hermitian adjoint (complex conjugate transpose)
$\mathbf{I}_n$	Identity matrix, $n \times n$
$\Im$	Imaginary
$\sim$	On the order of
$\Re$	Real
T	Transpose

A.2 Abbreviations

AOA	Angle of arrival
AOB	Angle of bearing
CRLB	Cramer-Rao lower bound
FI	Fisher information
LOS	Line of sight
MLE	Maximum likelihood estimator
MSE	Mean-square error
PDF	Probability density function
SQRTCRLB	Square root of the Cramer-Rao lower bound
2D	Two dimensions or two-dimensional
3D	Three dimensions or three-dimensional

Appendix B. Derivatives of Covariance Matrix and Mean

In order to calculate the FI matrix (equation (5)), we need the derivatives of the covariance matrix $\mathbf{C}$ and the mean vector $\boldsymbol{\mu}$ with respect to the unknown parameters $\boldsymbol{\Theta} = \left[\varphi\ \theta\ r\ \sigma_{\mathrm{N}}^2\ l\ \varsigma^2\ \chi\right]^{\mathrm{T}}$. The dependence of $\mathbf{C}$ and $\boldsymbol{\mu}$ on these parameters is given in section 4.1. The derivatives of the components of the covariance matrix (C_{ii} and $C_{ij}, i \neq j$) and mean vector (μ_i) with respect to these parameters are given in the following subsections.

B.1 Unknown Parameter φ

The derivatives with respect to the azimuth φ are

$$\frac{\partial C_{ii}}{\partial \varphi} = 0 \tag{B-1}$$

$$\frac{\partial C_{ij}}{\partial \varphi} = \mathrm{i}\,\frac{\partial \phi_{ij}}{\partial \varphi}\,C_{ij}\,,\ i \neq j \tag{B-2}$$

$$\frac{\partial \mu_i}{\partial \varphi} = \mathrm{i}\,\frac{\partial \phi_i}{\partial \varphi}\,\mu_i\,, \tag{B-3}$$

where

$$\frac{\partial \phi_i}{\partial \varphi} = k\left(-x_i' \sin\varphi \sin\theta + y_i' \cos\varphi \sin\theta\right) \tag{B-4}$$

$$\frac{\partial \phi_{ij}}{\partial \varphi} = \frac{\partial \phi_i}{\partial \varphi} - \frac{\partial \phi_j}{\partial \varphi}\,. \tag{B-5}$$

B.2 Unknown Parameter θ

The derivatives with respect to the zenith (declination) θ are

$$\frac{\partial C_{ii}}{\partial \theta} = 0 \tag{B-6}$$

$$\frac{\partial C_{ij}}{\partial \theta} = \mathrm{i}\,\frac{\partial \phi_{ij}}{\partial \theta}\,C_{ij}\,,\ i \neq j \tag{B-7}$$

$$\frac{\partial \mu_i}{\partial \theta} = \mathrm{i}\,\frac{\partial \phi_i}{\partial \theta}\,\mu_i\,, \tag{B-8}$$

where

$$\frac{\partial \phi_i}{\partial \theta} = -k \left(x_i' \cos\varphi \cos\theta + y_i' \sin\varphi \cos\theta - z_i' \sin\theta \right) \tag{B-9}$$

$$\frac{\partial \phi_{ij}}{\partial \theta} = \frac{\partial \phi_i}{\partial \theta} - \frac{\partial \phi_j}{\partial \theta} \,. \tag{B-10}$$

B.3 Unknown Parameter r

The derivatives with respect to the propagation distance r are

$$\frac{\partial C_{ii}}{\partial r} = -\frac{\partial \tilde{\mu}^2}{\partial r} \tag{B-11}$$

$$\frac{\partial C_{ij}}{\partial r} = \left[-p_0^2 \, \alpha(\rho_{ij}) \, e^{-\alpha(\rho_{ij}) \, r} - \frac{\partial \tilde{\mu}^2}{\partial r} \right] e^{\mathrm{i}\phi_{ij}} + \mathrm{i} \, \frac{\partial \phi_{ij}}{\partial r} \, C_{ij} \,, \; i \neq j \tag{B-12}$$

$$\frac{\partial \mu_i}{\partial r} = \frac{\partial \tilde{\mu}}{\partial r} \, e^{\mathrm{i}\phi_i} + \mathrm{i} \, \frac{\partial \phi_i}{\partial r} \, \mu_i \,, \tag{B-13}$$

where

$$\frac{\partial \tilde{\mu}^2}{\partial r} = -\alpha(\infty) \, \tilde{\mu}^2 \tag{B-14}$$

$$\frac{\partial \tilde{\mu}}{\partial r} = -\gamma \tilde{\mu} \tag{B-15}$$

$$\frac{\partial \phi_i}{\partial r} = k \tag{B-16}$$

$$\frac{\partial \phi_{ij}}{\partial r} = 0 \,. \tag{B-17}$$

B.4 Unknown Parameter for Noise

We can treat either the noise variance (σ_{N}^2) or the signal-to-noise ratio (SNR) as the unknown. First let us suppose that σ_{N}^2 is the unknown. Then

$$\frac{\partial C_{ii}}{\partial \sigma_{\mathrm{N}}^2} = 1 \tag{B-18}$$

$$\frac{\partial C_{ij}}{\partial \sigma_{\mathrm{N}}^2} = 0 \,, \; i \neq j \tag{B-19}$$

$$\frac{\partial \mu_i}{\partial \sigma_{\mathrm{N}}^2} = 0 \,. \tag{B-20}$$

Alternatively, we can take the SNR as the unknown. Recall that $\mathrm{SNR} = p_0^2/\sigma_{\mathrm{N}}^2$. Let Θ be the parameter symbol for the SNR. Then

$$\frac{\partial C_{ii}}{\partial \Theta} = \frac{\partial \sigma_{\mathrm{N}}^2}{\partial \Theta} \tag{B-21}$$

$$\frac{\partial C_{ij}}{\partial \Theta} = 0\,,\ i \neq j \tag{B-22}$$

$$\frac{\partial \mu_i}{\partial \Theta} = 0\,, \tag{B-23}$$

where

$$\frac{\partial \sigma_{\mathrm{N}}^2}{\partial \Theta} = -\frac{p_0^2}{\Theta^2} = -\frac{\sigma_{\mathrm{N}}^2}{\Theta}\,. \tag{B-24}$$

B.5 Unknown Turbulence Parameters

Consider the derivatives with respect to the turbulence parameters l (the length scale) and ς^2 (the index-of-refraction variance). Let $\Theta \in \left[l\,, \varsigma^2\right]$ be the unknown parameter. Then

$$\frac{\partial C_{ii}}{\partial \Theta} = -\frac{\partial \tilde{\mu}^2}{\partial \Theta} \tag{B-25}$$

$$\frac{\partial C_{ij}}{\partial \Theta} = \left[-p_0^2\, r\, \frac{\partial \alpha(\rho_{ij})}{\partial \Theta}\, e^{-\alpha(\rho_{ij})\, r} - \frac{\partial \tilde{\mu}^2}{\partial \Theta}\right] e^{\mathrm{i}\phi_{ij}} \tag{B-26}$$

$$\frac{\partial \mu_i}{\partial \Theta} = \frac{\partial \tilde{\mu}}{\partial \Theta}\, e^{\mathrm{i}\phi_i}\,, \tag{B-27}$$

where

$$\frac{\partial \tilde{\mu}^2}{\partial \Theta} = -r\, \frac{\partial \alpha(\infty)}{\partial \Theta}\, \tilde{\mu}^2 \tag{B-28}$$

$$\frac{\partial \tilde{\mu}}{\partial \Theta} = -\frac{r}{2}\, \frac{\partial \alpha(\infty)}{\partial \Theta}\, \tilde{\mu}\,. \tag{B-29}$$

Recall that $\alpha(\rho) = 2\pi k^2 \left[f(0) - f(\rho)\right]$, where f is the 2D correlation function for either a scalar or vector von Kármán spectrum as given in equations (18) and (19), respectively. The derivatives of f_s and f_v with respect to l and ς^2 are given in the following appendix.

Appendix C. Derivatives of $f(\rho)$ with respect to ς^2 and l

The scalar and vector 2D correlation functions, f_s and f_v, are given, respectively, in equations (18) and (19). In this section we calculate the derivatives of f_s and f_v with respect to the index-of-refraction variance ς^2 and with respect to the turbulence length scale l. The limits of $f(\rho)$, for $\rho \to 0$ and $\rho \to \infty$, are also calculated as well as their derivatives.

C.1 Derivative of $f(\rho)$ with respect to ς^2

The derivative of f, where f is either f_s or f_v, with respect to the index-of-refraction variance ς^2 is

$$\frac{\partial f}{\partial \varsigma^2} = \frac{f}{\varsigma^2}\,. \tag{C-30}$$

C.2 Derivative of $f(\rho)$ with respect to l, $\rho \neq 0$

The derivative of the scalar 2D correlation function $f_s(\rho)$, for $\rho \neq 0$, with respect to the turbulence length scale l is given by

$$\begin{aligned}
\frac{\partial f_s}{\partial l} &= \frac{\partial}{\partial l}\left[\frac{2\varsigma^2}{\sqrt{\pi}\,\Gamma(1/3)}\left(\frac{\rho}{2}\right)^{5/6} l^{1/6} K_{5/6}\left(\frac{\rho}{l}\right)\right] \\
&= \frac{2\varsigma^2}{\sqrt{\pi}\,\Gamma(1/3)}\left(\frac{\rho}{2}\right)^{5/6}\left[\frac{1}{6} l^{-5/6} K_{5/6}\left(\frac{\rho}{l}\right) - \rho\, l^{-11/6} K'_{5/6}\left(\frac{\rho}{l}\right)\right] \\
&= \frac{2\varsigma^2}{\sqrt{\pi}\,\Gamma(1/3)}\left(\frac{\rho}{2}\right)^{5/6}\left\{\frac{1}{6} l^{-5/6} K_{5/6}\left(\frac{\rho}{l}\right) + \frac{\rho}{2} l^{-11/6}\left[K_{1/6}\left(\frac{\rho}{l}\right) + K_{11/6}\left(\frac{\rho}{l}\right)\right]\right\} \\
&= \frac{2\varsigma^2}{\sqrt{\pi}\,\Gamma(1/3)}\left(\frac{\rho}{2l}\right)^{5/6}\left\{\frac{1}{6} K_{5/6}\left(\frac{\rho}{l}\right) + \frac{\rho}{2l}\left[K_{1/6}\left(\frac{\rho}{l}\right) + K_{11/6}\left(\frac{\rho}{l}\right)\right]\right\} \\
&= \frac{2\varsigma^2}{\sqrt{\pi}\,\Gamma(1/3)}\left(\frac{\rho}{2l}\right)^{5/6}\left[K_{5/6}\left(\frac{\rho}{l}\right) + \frac{\rho}{l} K_{1/6}\left(\frac{\rho}{l}\right)\right]\,.
\end{aligned} \tag{C-31}$$

In going from the second line to the third line and from the forth line to the fifth, the recursion relationships

$$K_{\nu-1}(x) + K_{\nu+1}(x) = -2K'_\nu(x) \tag{C-32}$$

$$K_{\nu-1}(x) - K_{\nu+1}(x) = -\frac{2\nu}{x} K_\nu(x) \tag{C-33}$$

and the relationship

$$K_\nu(x) = K_{-\nu}(x) \tag{C-34}$$

have been used, (see, for example, Arfken [13] or Gradshteyn and Ryzhik [14]). The intermediate algebraic steps are not shown.

The derivative of the vector 2D correlation function $f_v(\rho)$, for $\rho \neq 0$, with respect to the turbulence length scale l may be written in the form

$$\begin{aligned}
\frac{\partial f_v}{\partial l} &= \frac{\partial f_s}{\partial l} - \frac{2\varsigma^2}{\sqrt{\pi}\,\Gamma(1/3)}\left(\frac{\rho}{2}\right)^{11/6}\frac{\partial}{\partial l}\left[l^{-5/6}K_{1/6}\left(\frac{\rho}{l}\right)\right] \\
&= \frac{\partial f_s}{\partial l} - \frac{2\varsigma^2}{\sqrt{\pi}\,\Gamma(1/3)}\left(\frac{\rho}{2}\right)^{11/6}\left[-\frac{5}{6}l^{-11/6}K_{1/6}\left(\frac{\rho}{l}\right) - \rho\, l^{-17/6}K'_{1/6}\left(\frac{\rho}{l}\right)\right] \\
&= \frac{\partial f_s}{\partial l} - \frac{2\varsigma^2}{\sqrt{\pi}\,\Gamma(1/3)}\left(\frac{\rho}{2l}\right)^{11/6}\left\{-\frac{5}{6}K_{1/6}\left(\frac{\rho}{l}\right) + \frac{\rho}{2l}\left[K_{5/6}\left(\frac{\rho}{l}\right) + K_{7/6}\left(\frac{\rho}{l}\right)\right]\right\} \\
&= \frac{2\varsigma^2}{\sqrt{\pi}\,\Gamma(1/3)}\left(\frac{\rho}{2l}\right)^{5/6}\left\{\frac{1}{6}K_{5/6}\left(\frac{\rho}{l}\right) + \frac{\rho}{2l}\left[\frac{11}{6}K_{1/6}\left(\frac{\rho}{l}\right) + K_{11/6}\left(\frac{\rho}{l}\right)\right]\right. \\
&\qquad\qquad \left. - \left(\frac{\rho}{2l}\right)^2\left[K_{5/6}\left(\frac{\rho}{l}\right) + K_{7/6}\left(\frac{\rho}{l}\right)\right]\right\} \\
&= \frac{2\varsigma^2}{\sqrt{\pi}\,\Gamma(1/3)}\left(\frac{\rho}{2l}\right)^{5/6}\left\{\left[1 - \frac{1}{2}\left(\frac{\rho}{l}\right)^2\right]K_{5/6}\left(\frac{\rho}{l}\right) + \frac{4\rho}{3l}K_{1/6}\left(\frac{\rho}{l}\right)\right\}.
\end{aligned} \tag{C-35}$$

Again the recursion relationships have been used in going from the second line to the third and from the forth line to the fifth. The intermediate algebraic steps are not shown.

C.3 Evaluation of $f(0)$ and Derivative of $f(0)$ with respect to l

We wish to evaluate $f_s(\rho)$ and $f_v(\rho)$ in the limit that $\rho \to 0$. Consider

$$f_s(0) = \lim_{\rho\to 0} C\left(\frac{\rho}{l}\right)^{5/6}K_{5/6}\left(\frac{\rho}{l}\right) \tag{C-36}$$

$$f_v(0) = \lim_{\rho\to 0} C\left(\frac{\rho}{l}\right)^{5/6}\left[K_{5/6}\left(\frac{\rho}{l}\right) - \frac{\rho}{2l}K_{1/6}\left(\frac{\rho}{l}\right)\right], \tag{C-37}$$

where

$$C \equiv \frac{2\varsigma^2 l}{2^{5/6}\sqrt{\pi}\,\Gamma(1/3)}. \tag{C-38}$$

For $x \in \Re$ and $\nu > 0$, (see, e.g., Arfken [13]),

$$\lim_{x\to 0} K_\nu(x) = \frac{\Gamma(\nu)2^{\nu-1}}{x^\nu}. \tag{C-39}$$

Therefore, for $x \in \Re$ and $\nu > 0$,

$$\lim_{x \to 0} x^{\lambda} K_{\nu}(x) = \begin{cases} \infty & \text{if } \lambda < \nu\,, \\ 2^{\nu-1}\Gamma(\nu) & \text{if } \lambda = \nu\,, \\ 0 & \text{if } \lambda > \nu\,. \end{cases} \tag{C-40}$$

It follows that

$$f_s(0) = C\, 2^{-1/6}\, \Gamma\left(\frac{5}{6}\right) = \frac{\varsigma^2 l\, \Gamma\left(\frac{5}{6}\right)}{\sqrt{\pi}\, \Gamma\left(\frac{1}{3}\right)} = \frac{\varsigma^2 l}{\beta\left(\frac{1}{2}, \frac{1}{3}\right)} = f_v(0)\,, \tag{C-41}$$

where β is the beta function, $\beta(x, y) = \Gamma(x)\Gamma(y)/\Gamma(x + y)$. Thus

$$\frac{\partial f(0)}{\partial l} = \frac{\varsigma^2}{\beta\left(\frac{1}{2}, \frac{1}{3}\right)} = \frac{f(0)}{l}\,. \tag{C-42}$$

C.4 Evaluation of $f(\infty)$

We wish to evaluate $f_s(\rho)$ and $f_v(\rho)$ in the limit $\rho \to \infty$. We note that in the asymptotic expansion of $K_{\nu}(x)$, $x \in \Re$, the leading term is proportional to $e^{-x}/\sqrt{x}$. As such the exponential term will dominate in f_s and f_v. Hence

$$f_s(\infty) = f_v(\infty) = 0\,. \tag{C-43}$$

We refer the reader to [13] and [14] for comments regarding the asymptotic expansion of $K_{\nu}(x)$.

Appendix D. Simple Two-Element Array Model

Consider the simple case of a two-element array, and let Θ_λ and Θ_ν be unknown parameters. Let us write the covariance matrix as

$$\mathbf{C} = \begin{bmatrix} a & b \\ b^* & a \end{bmatrix}, \tag{D-1}$$

where $b = \beta e^{i\phi_{12}}$ and $a,\ \beta \in \Re$. Let us write the mean vector as

$$\boldsymbol{\mu} = \begin{bmatrix} \mu_1 \\ \mu_2 \end{bmatrix} = \tilde{\mu} \begin{bmatrix} e^{i\phi_1} \\ e^{i\phi_2} \end{bmatrix}. \tag{D-2}$$

It follows that

$$\begin{aligned} \operatorname{tr}\left(\mathbf{C}^{-1}\frac{\partial \mathbf{C}}{\partial \Theta_\lambda}\mathbf{C}^{-1}\frac{\partial \mathbf{C}}{\partial \Theta_\nu}\right) &= \frac{2}{(\det \mathbf{C})^2}\,\Re\left[\left(a\frac{\partial a}{\partial \Theta_\lambda} - b^*\frac{\partial b}{\partial \Theta_\lambda}\right)\left(a\frac{\partial a}{\partial \Theta_\nu} - b^*\frac{\partial b}{\partial \Theta_\nu}\right)\right. \\ &\qquad \left. + \left(a\frac{\partial b}{\partial \Theta_\lambda} - b\frac{\partial a}{\partial \Theta_\lambda}\right)\left(a\frac{\partial b^*}{\partial \Theta_\nu} - b^*\frac{\partial a}{\partial \Theta_\nu}\right)\right] \qquad \text{(D-3)} \\ &= \frac{2}{(a^2-\beta^2)^2}\left[(a^2+\beta^2)\left(\frac{\partial a}{\partial \Theta_\lambda}\frac{\partial a}{\partial \Theta_\nu} + \frac{\partial \beta}{\partial \Theta_\lambda}\frac{\partial \beta}{\partial \Theta_\nu}\right)\right. \\ &\qquad \left. - 2a\beta\left(\frac{\partial a}{\partial \Theta_\lambda}\frac{\partial \beta}{\partial \Theta_\nu} + \frac{\partial a}{\partial \Theta_\nu}\frac{\partial \beta}{\partial \Theta_\lambda}\right) + \beta^2\left(a^2-\beta^2\right)\frac{\partial \phi_{12}}{\partial \Theta_\lambda}\frac{\partial \phi_{12}}{\partial \Theta_\nu}\right] \qquad \text{(D-4)} \end{aligned}$$

and

$$\begin{aligned} \Re\left(\frac{\partial \boldsymbol{\mu}}{\partial \Theta_\lambda}^{\dagger}\mathbf{C}^{-1}\frac{\partial \boldsymbol{\mu}}{\partial \Theta_\nu}\right) &= \Re\left\{\frac{1}{\det \mathbf{C}}\left[\frac{\partial \mu_1^*}{\partial \Theta_\lambda}\left(a\frac{\partial \mu_1}{\partial \Theta_\nu} - b\frac{\partial \mu_2}{\partial \Theta_\nu}\right) + \frac{\partial \mu_2^*}{\partial \Theta_\lambda}\left(a\frac{\partial \mu_2}{\partial \Theta_\nu} - b^*\frac{\partial \mu_1}{\partial \Theta_\nu}\right)\right]\right\} \qquad \text{(D-5)} \\ &= \frac{1}{a^2-\beta^2}\left\{2(a-\beta)\frac{\partial \tilde{\mu}}{\partial \Theta_\lambda}\frac{\partial \tilde{\mu}}{\partial \Theta_\nu} + \tilde{\mu}^2\left[a\left(\frac{\partial \phi_1}{\partial \Theta_\lambda}\frac{\partial \phi_1}{\partial \Theta_\nu} + \frac{\partial \phi_2}{\partial \Theta_\lambda}\frac{\partial \phi_2}{\partial \Theta_\nu}\right)\right.\right. \\ &\qquad \left.\left. - \beta\left(\frac{\partial \phi_1}{\partial \Theta_\lambda}\frac{\partial \phi_2}{\partial \Theta_\nu} + \frac{\partial \phi_1}{\partial \Theta_\nu}\frac{\partial \phi_2}{\partial \Theta_\lambda}\right)\right]\right\}. \qquad \text{(D-6)} \end{aligned}$$

Recall for a Gaussian process, the FI is given by equation (5). Thus, for $\xi = \lambda$ or ν,

$$J_{\xi\xi} = \frac{2M}{(a^2-\beta^2)^2}\left\{(a^2+\beta^2)\left[\left(\frac{\partial a}{\partial\Theta_\xi}\right)^2+\left(\frac{\partial\beta}{\partial\Theta_\xi}\right)^2\right]-4a\beta\frac{\partial a}{\partial\Theta_\xi}\frac{\partial\beta}{\partial\Theta_\xi}+\beta^2\left(a^2-\beta^2\right)\left(\frac{\partial\phi_{12}}{\partial\Theta_\xi}\right)^2\right\}$$
$$+\frac{2M}{a^2-\beta^2}\left\{2\left(a-\beta\right)\left(\frac{\partial\tilde{\mu}}{\partial\Theta_\xi}\right)^2+a\tilde{\mu}^2\left[\left(\frac{\partial\phi_1}{\partial\Theta_\xi}\right)^2+\left(\frac{\partial\phi_2}{\partial\Theta_\xi}\right)^2\right]-2\beta\tilde{\mu}^2\frac{\partial\phi_1}{\partial\Theta_\xi}\frac{\partial\phi_2}{\partial\Theta_\xi}\right\}. \quad \text{(D-7)}$$

For the special case when $\partial a/\partial\Theta_\lambda = \partial\beta/\partial\Theta_\lambda = \partial\tilde{\mu}/\partial\Theta_\lambda = 0$, but there are no restrictions on the derivatives with respect to Θ_ν,

$$J_{\lambda\lambda} = \frac{2M\beta^2}{a^2-\beta^2}\left(\frac{\partial\phi_{12}}{\partial\Theta_\lambda}\right)^2+\frac{2M\tilde{\mu}^2}{a^2-\beta^2}\left\{a\left[\left(\frac{\partial\phi_1}{\partial\Theta_\lambda}\right)^2+\left(\frac{\partial\phi_2}{\partial\Theta_\lambda}\right)^2\right]-2\beta\frac{\partial\phi_1}{\partial\Theta_\lambda}\frac{\partial\phi_2}{\partial\Theta_\lambda}\right\}, \quad \text{(D-8)}$$

$$J_{\lambda\nu} = \frac{2M\beta^2}{a^2-\beta^2}\frac{\partial\phi_{12}}{\partial\Theta_\lambda}\frac{\partial\phi_{12}}{\partial\Theta_\nu}+\frac{2M\tilde{\mu}^2}{a^2-\beta^2}\left[a\left(\frac{\partial\phi_1}{\partial\Theta_\lambda}\frac{\partial\phi_1}{\partial\Theta_\nu}+\frac{\partial\phi_2}{\partial\Theta_\lambda}\frac{\partial\phi_2}{\partial\Theta_\nu}\right)-\beta\left(\frac{\partial\phi_1}{\partial\Theta_\lambda}\frac{\partial\phi_2}{\partial\Theta_\nu}+\frac{\partial\phi_1}{\partial\Theta_\nu}\frac{\partial\phi_2}{\partial\Theta_\lambda}\right)\right], \quad \text{(D-9)}$$

and $J_{\nu\nu}$ is given by equation (D-7) with $\xi = \nu$.

References

1. B.-G. Song and J. A. Ritcey, "Angle of arrival estimation of plane waves propagating in random media," J. Acoust. Soc. Am. **99**, 1370–1379 (1996).

2. D. K. Wilson, "Performance bounds for acoustic direction-of-arrival arrays operating in atmospheric turbulence," J. Acoust. Soc. Am. **103**, 1306–1319 (1998).

3. S. M. Kay, *Fundamentals of Statistical Signal Processing: Estimation Theory*, PTR Prentice Hall, Englewood Cliffs, NJ (1993).

4. L. L. Scharf, *Statistical Signal Process: Detection, Estimation, and Time Series Analysis*, Addison-Wesley, Reading, MA (1991).

5. V. E. Ostashev, *Acoustics in Moving Inhomogeneous Media*, E & FN Spon, London (1997).

6. D. K. Wilson, "Atmospheric Effects on Acoustic Arrays: A Broad Perspective From Models," IRIS Symposium on Battlefield Acoustics and Seismics, Laurel, MD (1999).

7. V. E. Ostashev and D. K. Wilson, "Relative Contributions from Temperature and Wind Velocity Fluctuations to the Statistical Moments of a Sound Field in a Turbulent Atmosphere," Acustica **86**, 260–268 (2000).

8. D. K. Wilson, "A turbulence spectral model for sound propagation in the atmosphere that incorporates shear and buoyancy forcings," J. Acoust. Soc. Am. **108**, 2021–2038 (2000).

9. R. O. Nielsen, "Estimation of Azimuth and Elevation Angles for a Plane Wave Sine Wave with a 3-D Array," IEEE Trans. Sig. Proc. **42**, 3274–3276 (1994).

10. R. O. Nielsen, "Azimuth and Elevation Angle Estimation with a Three-Dimensional Array," IEEE J. Ocean Engineering **19**, 84–86 (1994).

11. A. N. Mirkin and L. H. Sibul, "Cramer-Rao Bounds on Angle

Estimation with a Two-Dimensional Array," IEEE Trans. Sig. Proc. **39**, 515–517 (1991).

12. Y. Hua and T. K. Sarkar, "A Note on the Cramer-Rao Bound for 2-D Direction Finding Based on 2-D Array," IEEE Trans. on Sig. Proc. **39**, 1215–1218 (1991).

13. G. Arfken, *Mathematical Methods for Physicists*, Academic Press, Inc., Orlando, FL (1985).

14. I. S. Gradshteyn and I. M. Ryzhik, *Table of Integrals, Series, and Products*, Academic Press, Inc., Orlando, FL (1980).

Distribution

Admnstr
Defns Techl Info Ctr
ATTN DTIC-OCP
8725 John J Kingman Rd Ste 0944
FT Belvoir VA 22060-6218

DARPA
ATTN S Welby
3701 N Fairfax Dr
Arlington VA 22203-1714

Mil Asst for Env Sci Ofc of the Undersec
of Defns for Rsrch & Engrg R&AT E LS
Pentagon Rm 3D129
Washington DC 20301-3080

Ofc of the Secy of Defns
ATTN ODDRE (R&AT)
The Pentagon
Washington DC 20301-3080

AMCOM MRDEC
ATTN AMSMI-RD W C McCorkle
Redstone Arsenal AL 35898-5240

Natl Ground Intllgnc Ctr
Army Foreign Sci Tech Ctr
ATTN CM
220 7th Stret NE
Charlottesville VA 22901-5396

US Army TRADOC
Battle Lab Integration & Techl Dirctrt
ATTN ATCD-B
FT Monroe VA 23651-5850

US Army TRADOC
Battle Lab Integration & Techl Dirctrt
ATTN ATCD-B J A Klevecz
FT Monroe VA 23651-5850

US Military Acdmy
Mathematical Sci Ctr of Excellence
ATTN MADN-MATH MAJ M Johnson
Thayer Hall
West Point NY 10996-1786

Dir for MANPRINT
Ofc of the Deputy Chief of Staff for Prsnnl
ATTN J Hiller
The Pentagon Rm 2C733
Washington DC 20301-0300

SMC/CZA
2435 Vela Way Ste 1613
El Segundo CA 90245-5500

TECOM
ATTN AMSTE-CL
Aberdeen Proving Ground MD 21005-5057

US Army ARDEC
ATTN AMSTA-AR-TD
Bldg 1
Picatinny Arsenal NJ 07806-5000

US Army CRREL
ATTN CRREL-GP R Detsch
72 Lyme Rd
Hanover NH 03755-1290

US Army Dugway Proving Ground
ATTN STEDP 3
ATTN STEDP-MT-DA-L-3
ATTN STEDP-MT-M Bowers
Dugway UT 84022-5000

US Army Field Artillery Schl
ATTN ATSF-TSM-TA
FT Sill OK 73503-5000

US Army Infantry
ATTN ATSH-CD-CS-OR E Dutoit
FT Benning GA 30905-5090

US Army Info Sys Engrg Cmnd
ATTN AMSEL-IE-TD F Jenia
FT Huachuca AZ 85613-5300

US Army Materiel Sys Anal Actvty
ATTN AMXSY-CS Bradley
Aberdeen Proving Ground MD 21005-5071

US Army Natick RDEC Acting Techl Dir
ATTN SBCN-T P Brandler
Natick MA 01760-5002

Distribution (cont'd)

US Army OEC
ATTN CSTE-AEC-FSE
4501 Ford Ave Park Center IV
Alexandria VA 22302-1458

US Army Simulation Train & Instrmntn Cmnd
ATTN AMSTI-CG M Macedonia
ATTN J Stahl
12350 Research Parkway
Orlando FL 32826-3726

US Army TACOM-ARDEC
ATTN AMSTA-AR-WEL-TL
Bldg 59 Phillips Rd
Picatinny Arsenal NJ 07806-5000

US Army Tank-Automtv Cmnd RDEC
ATTN AMSTA-TR J Chapin
Warren MI 48397-5000

US Army TRADOC
ATTN ATCD-FA
FT Monroe VA 23651-5170

US Army TRADOC Anal Cmnd—WSMR
ATTN ATRC-WSS-R
White Sands Missile Range NM 88002

Nav Air War Ctr Wpn Div
ATTN CMD 420000D C0245 A Shlanta
1 Admin Cir
China Lake CA 93555-6001

Nav Surfc Warfare Ctr
ATTN Code B07 J Pennella
17320 Dahlgren Rd Bldg 1470 Rm 1101
Dahlgren VA 22448-5100

Nav Surfc Weapons Ctr
ATTN Code G63
Dahlgren VA 22448-5000

AFCCC/DOC
ATTN Glauber
151 Patton Ave Rm 120
Asheville NC 28801-5002

Hdqtrs AFWA/DNX
106 Peacekeeper Dr Ste 2N3
Offutt AFB NE 68113-4039

USAF Rome Lab Tech
ATTN Corridor W Ste 262 RL SUL
26 Electr Pkwy Bldg 106
Griffiss AFB NY 13441-4514

Univ of Mississippi NCPA
ATTN H E Bass
University MS 38577

Hicks & Assoc Inc
ATTN G Singley III
1710 Goodrich Dr Ste 1300
McLean VA 22102

Natl Ctr for Atmos Rsrch
ATTN NCAR Library Serials
PO Box 3000
Boulder CO 80307-3000

Director
US Army Rsrch Lab
ATTN AMSRL-RO-D JCI Chang
ATTN AMSRL-RO-EN W D Bach
PO Box 12211
Research Triangle Park NC 27709

US Army Rsrch Lab
ATTN AMSRL-CI-E J Mercurio
ATTN AMSRL-CI-EE P Clark
ATTN AMSRL-CI-EE D K Wilson (5 copies)
ATTN AMSRL-CI-IS-R Mail & Records Mgmt
ATTN AMSRL-CI-IS-T Techl Pub (2 copies)
ATTN AMSRL-CI-OK-TL Techl Lib (2 copies)
ATTN AMSRL-D D R Smith
ATTN AMSRL-DD J M Miller
ATTN AMSRL-SE-EE Z G Sztankay
ATTN AMSRL-SE-SA J Eicke
ATTN AMSRL-SE-SA N Srour
ATTN AMSRL-SE-SA T Pham
ATTN AMSRL-CI-EE S L Collier (30 copies)

REPORT DOCUMENTATION PAGE

Form Approved
OMB No. 0704-0188

1. AGENCY USE ONLY *(Leave blank)*	2. REPORT DATE	3. REPORT TYPE AND DATES COVERED
	February 2002	Final, 1/00–1/01

4. TITLE AND SUBTITLE Performance Bounds on Atmospheric Acoustic Sensor Arrays Operating in a Turbulent Medium

5. FUNDING NUMBERS
DA PR: B53A
PE: 61102A

6. AUTHOR(S) Sandra L. Collier and D. Keith Wilson

7. PERFORMING ORGANIZATION NAME(S) AND ADDRESS(ES)
U.S. Army Research Laboratory
Attn: AMSRL-CI-EP email: scollier@arl.army.mil
2800 Powder Mill Road
Adelphi, MD 20783-1197

8. PERFORMING ORGANIZATION REPORT NUMBER
ARL-TR-2426

9. SPONSORING/MONITORING AGENCY NAME(S) AND ADDRESS(ES)
U.S. Army Research Laboratory
2800 Powder Mill Road
Adelphi, MD 20783-1197

10. SPONSORING/MONITORING AGENCY REPORT NUMBER

11. SUPPLEMENTARY NOTES
ARL PR: OFEJ60
AMS code: 61110253A11

12a. DISTRIBUTION/AVAILABILITY STATEMENT Approved for public release; distribution unlimited.

12b. DISTRIBUTION CODE

13. ABSTRACT *(Maximum 200 words)*
The performance bounds of an atmospheric acoustic array operating in a turbulent medium with fluctuations described by a von Kármán spectrum are investigated. This treatment considers a single monochromatic source and a line-of-sight propagation path. The primary interests are in calculating the Cramer-Rao lower bounds (CRLBs) of the azimuthal and zenith angles of arrival (AOAs) and in observing how these bounds change with the introduction of additional unknowns, such as the normalized propagation distance (to wavelength), turbulence parameters, and signal-to-noise ratio (SNR). In both two and three dimensions, the CRLBs of the AOAs increase significantly for large values of the index-of-refraction variance and normalized propagation distance. For small values of the index-of-refraction variance and normalized propagation distance, the SNR is the limiting factor. For the two-dimensional treatment, the estimate of the AOA will decouple from the estimates of the other parameters with the appropriate choice of array geometry. In three dimensions, again with an appropriate choice of array geometry, the estimates of the azimuth and zenith will decouple from the estimates of the other parameters, but because of the constraints of the turbulence model, they will remain coupled to one another.

14. SUBJECT TERMS Acoustic arrays, sound propagation, Fisher information, Cramer-Rao lower bound, random media

15. NUMBER OF PAGES 62

16. PRICE CODE

17. SECURITY CLASSIFICATION OF REPORT	18. SECURITY CLASSIFICATION OF THIS PAGE	19. SECURITY CLASSIFICATION OF ABSTRACT	20. LIMITATION OF ABSTRACT
Unclassified	Unclassified	Unclassified	SAR

NSN 7540-01-280-5500

Standard Form 298 (Rev. 2-89)
Prescribed by ANSI Std. Z39-18
298-102